International Journal of Thermal Sciences 157 (2020) 106500

Contents lists available at ScienceDirect

International Journal of Thermal Sciences

journal homepage: http://www.elsevier.com/locate/ijts

Experimental and numerical study of smoke behavior in high-rise stairwells with open and closed windows

Chan-Sol Ahn [a,b], Doo-Young Kim [b], Chanwoo Park [a], Min-Woo Kim [a], Taegun Kim [a], Boo-Hyoung Bang [c], Seongpil An [d,**], Alexander L. Yarin [e,***], Sam S. Yoon [a,*]

[a] School of Mechanical Engineering, Korea University, Seoul, 02841, South Korea
[b] Fire Research Center, Korea Institute of Civil Engineering and Building Technology, 283, Goyang-daero, Ilsanseo-gu, 10223, Goyang-si, South Korea
[c] Department of Energy Mechanical Engineering, Gyeonggi University of Science and Technology, 269, Gyeonggigwagidae-ro, Siheung-si, 15073, South Korea
[d] SKKU Advanced Institute of Nanotechnology (SAINT) and Department of Nano Engineering, Sungkyunkwan University (SKKU), Suwon, 16419, Republic of Korea
[e] Department of Mechanical & Industrial Engineering, University of Illinois at Chicago, 842 W. Taylor St., Chicago, 60607, USA

ARTICLE INFO

Keywords:
Smoke dynamics
High-rise stairwells
Turbulent plume
Flow visualization
Ventilation
Open-windows

ABSTRACT

This study numerically and experimentally investigates the transport phenomena in buoyancy-driven smoke inside stairwells in a high-rise building. Hot smoke is supplied at the bottom of a small-scale, 2-m high stairwell prototype, and the smoke velocity and temperature are measured and compared with the corresponding numerical results. For all-windows-closed cases, the Fire Dynamics Simulator (FDS) model is used to predict the smoke velocity and temperature fields, which are found to be in good agreement with the experimental data. Obstruction caused by the stairs is observed to slow the smoke flow, which results in staggering and repeated vortical flows in all stairwells, confirmed by flow visualization. The flow path lines and vortex formation of the smoke inside the stairwells are visualized using the laser-induced fluorescence (LIF) method; these vortical structures also corresponded to the results of FDS simulation. Furthermore, the effect of heating power (Q) is investigated in the range of 60–180 W for experiments and 1–4 kW for simulations. Both temperature and velocity increase with Q. Having one open window at various building heights is shown to have small effect on the overall smoke temperature, although having many open windows causes a temperature drop owing to the inflow of fresh, cool air. Having one open window at various building heights slightly slows the smoke velocity, although the velocity is significantly decreased when many windows are open. Therefore, the intake of fresh air slows the overall smoke dynamics. Moreover, the effect of Q in the range of 2–20 MW over building heights of 60, 120, and 240 m is numerically simulated. The rate at which the smoke reaches high elevations is determined for all-windows-closed and all-windows-open cases based on our parametric studies. The smoke rise time (t) is shown to be proportional to $\sim Q^{1/3}$ for all building heights, which is the same time scale as the one predicted by the plume theory. However, because of the complex internal geometry of confined buildings including stairwells and corridors, the magnitude of the smoke rise time for the building is much larger than that predicted by the plume theory. Therefore, the current experimental and numerical findings may be useful as design guidelines for building safety engineers.

1. Introduction

In the case of a building fire, toxic smoke poses greater danger to human lives than the fire itself because smoke can rapidly reach higher floors owing to its high mobility [1–3]. Therefore, it is critically important to understand the smoke dynamics under various fire scenarios considering the fire size and the status of windows, whether open or closed.

Smoke rise is a buoyancy-driven phenomenon caused by the expansion of hot smoke, which is lighter than the surrounding air. Therefore, the density difference between the hot smoke and the surrounding air enables the smoke to rise, which creates lower pressure

* Corresponding author.
** Corresponding author.
*** Corresponding author.
E-mail addresses: esan@skku.edu (S. An), ayarin@uic.edu (A.L. Yarin), skyoon@korea.ac.kr (S.S. Yoon).

https://doi.org/10.1016/j.ijthermalsci.2020.106500
Received 16 December 2019; Received in revised form 17 April 2020; Accepted 22 May 2020
Available online 16 June 2020

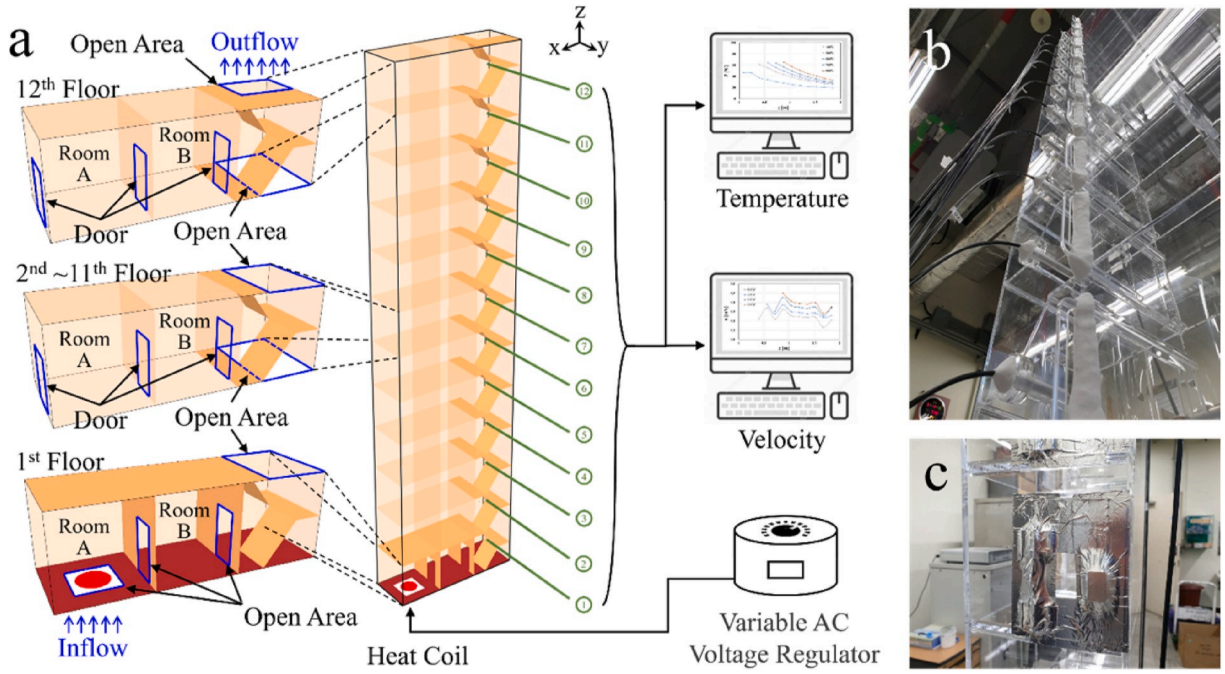

Fig. 1. (a) Detailed illustration of the high-rise building prototype used in the experiments. (b) Photograph of the prototype. The temperature and velocity sensors are inserted inside the stairwell column. (c) Sealed window attached to Room A.

near the heat source. As a result, relatively lower and higher pressure zones are formed at lower and higher locations of the building, respectively, when the heat source is located inside a building. This phenomenon, referred to as the "stack effect" [4–7], creates air suction at the bottom of the building, which supplies fresh air to enhance the fire intensity. Under this fire scenario, the status of doors and windows plays a vital role in the amount of fresh air taken in due to the suction power of the fire, which determines the overall smoke dynamics.

When a fire occurs under open-air conditions, the smoke dynamics can be well described by the plume theory [8–11] which has been validated against McCaffrey's experimental data [12]. However, fire in an actual confined-fire scenario is of greater interest. Thus, fires occurring in compartments, horizontal hallways, vertical shafts or lifts, ventilation systems, and atriums have been thoroughly studied by various investigators using simplified models [13–32]. Unfortunately, however, the smoke motion in a building fire is much more complex than that in a simple cylinder because the former involves motion around complex geometries such as, for example, stairwells, which are spiral in shape [33–46]. The presence of stairwells causes a spiral motion of the rising smoke and thus introduces the longer smoke pathway and greater drag on flow motion. This motion is further complicated with the presence, the number and location of open windows.

Sun et al. [34] conducted real-scale experiments on smoke dynamics in a six-story building including interior stairwells. The vortical motion of the rising smoke was observed, and the smoke temperature and velocity as functions of height were recorded. Ji et al. [35] introduced a 12-m building prototype to experimentally study smoke motion inside. They concluded that the smoke rise time with increasing height is inversely proportional to the 1/3 power of the heat release rate or the fire size. Li et al. [36] used a 12-m building prototype to study the smoke dynamics in the fire range of 12–94 kW with a window open in the neutral plane, at which the pressure inside the building is equal to the outside pressure. In their study, the smoke pressure was equal to the air pressure outside the building. Shi et al. [38] also used a 12-m building prototype to study the effect of the open-window location. Ji et al. [41] used the same 12-m building prototype to study the effects of vent locations, including bottom and top vents, and their effect on the burning rate of the fire. Ji et al. [40] studied the effect of open vents on the first, third, sixth, and ninth floors on the smoke temperature and rise time. Ji et al. [43,44] also investigated the effect of an open vent on smoke behavior, and Li et al. [45] numerically modeled the smoke dynamics inside a 35-m-high building using Fire Dynamics Simulators (FDS). Zhang et al. [46] also used FDS to simulate the smoke dynamics inside a 90-m-tall building.

Despite multiple experimental and numerical studies conducted on smoke motion inside a building with stairwells, a systematic study with different open-window scenarios in the various fire-size ranges has not been reported, especially for a building height greater than 100 m. A quantitative comparison of the effect of closed and open windows is of particular interest in studies of smoke dynamics for a building height greater than 200 m and is therefore, conducted in the present study. We also investigate whether the smoke rise time differs for various building heights, which would invalidate the 1/3 power scaling for different building sizes. A lab-scale prototype 2-m-tall building including stairwells is introduced to study the smoke dynamics experimentally, as shown in Fig. 1. This reduced scaling would produce much lower temperature and velocity than the actual flow characteristics. Nevertheless, this reduced-scale experiment has been commonly used as a benchmark case for numerical and theoretical modeling as the real large-scale fire experiment is extremely difficult to carry out. In addition, the results related to this 1/10-scale prototype are easily extrapolated to the actual scale using the scaling law provided by Ahn et al. [8–10]. Accordingly, the data from the small-scale experiment are going to be used as validation data for FDS (Fire Dynamics Simulators) numerical simulations. Upon validation, the use of FDS can be extended to real-scale fires for further investigation on realistic-scale building fires.

On the first floor of the prototype building, a heat source is installed with a heating power of 60–180 W; a sensor measuring the temperature and velocity of the rising smoke is installed on each of the twelve floors. The experimental results are compared and validated against the FDS numerical simulations and the numerical predictions are then extended to a fire size up to 20 MW, which is close to that in actual building fires. Based on these experimental and numerical results, empirical formulas describing the smoke rise time are suggested for cases with open and closed windows. The vortical motion of smoke arising from the spiral structure of the stairwells is evaluated using the laser-induced

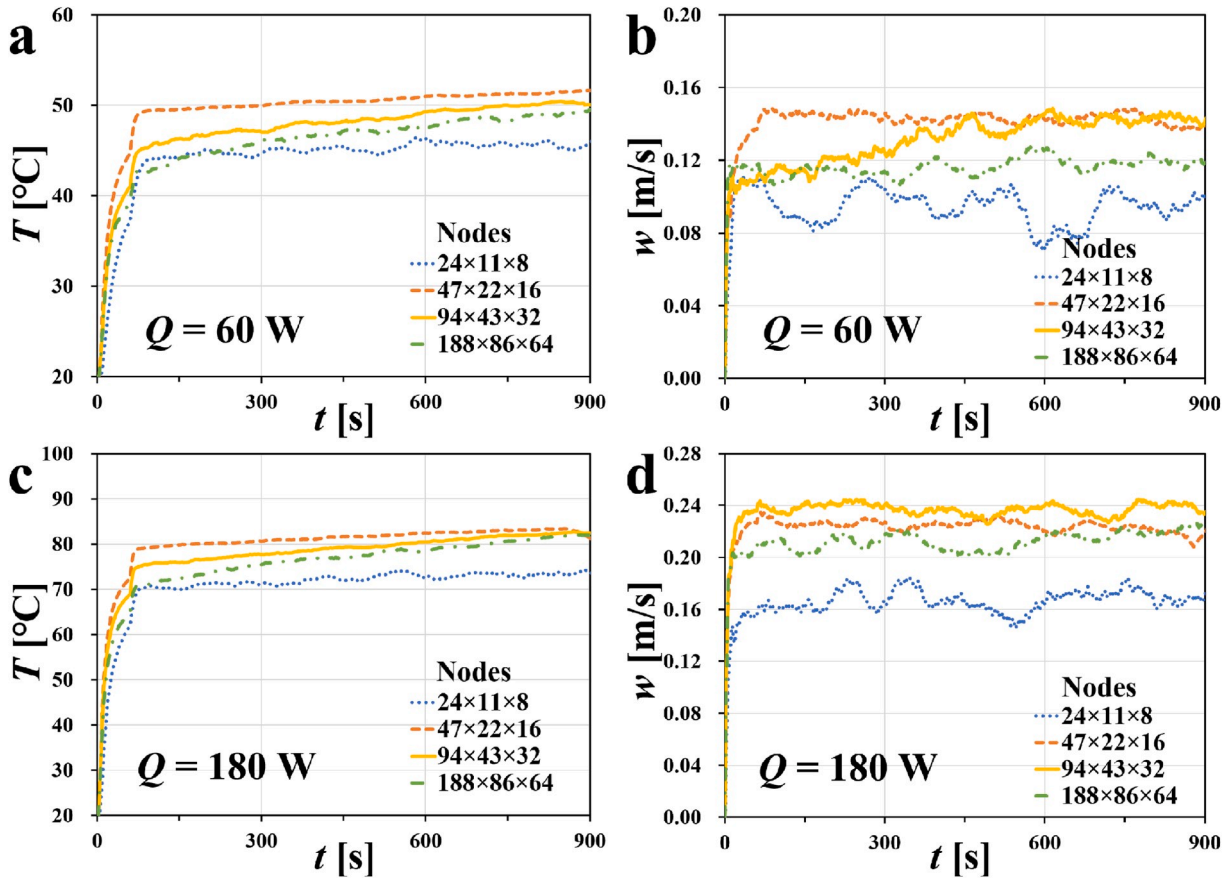

Fig. 2. Grid-refinement studies for (a, c) T, (b, d) w for the heating power $Q = 60$ W and 180 W, respectively, at $z = 0.17$ m in the stairwell with the surrounding temperature of $T_\infty = 20$ °C.

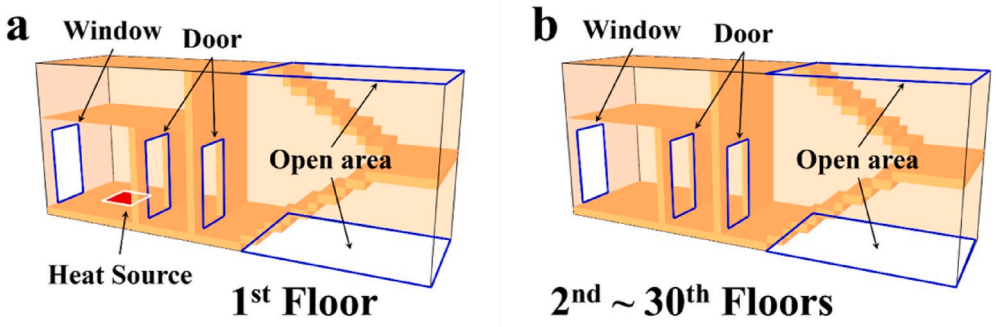

Fig. 3. Detailed structure of each floor of 60-m and 120-m buildings used for large-scale fire simulations ($2 \leq Q \leq 20$ MW).

fluorescence (LIF) technique.

2. Experiments

2.1. Experiment overview

Fig. 1 depicts the 2-m-tall, 12-floor building prototype used in the experiments, with exact dimensions of 0.5 m × 0.15 m × 2.0 m. The prototype was composed of transparent acrylic material to enable visualization of the rising smoke. The thickness of the acrylic material was 5 mm, and the thermal conductivity, specific heat, and density values were 0.2 W/m·K, 1.5 kJ/kg·K, and 1500 kg/m^3, respectively. The heat source (electric coil) was located at the bottom of the first floor, from which the smoke was supplied through a hole 5 cm in diameter. The smoke was generated by a smoke generator (1.2 kW max, liquid consumption 72 ml/min, FLG-5 Heavy, CHAUVET DJ, Hurricane 1200) and passed through an electric coil, which provided heat. The smoke was highly visible when exposed to laser light (wavelength 532 nm, Max. Power 3 W). An electric coil was situated directly below the hole and controlled by a variable alternating current (AC) voltage regulator. The supplied power (P) to the coil can be calculated as $P = I{\cdot}V$. The coil was encased by a metal cylinder that was fully insulated to prevent heat losses. As shown in Fig. 1a, each floor included Rooms A and B connected through an open door, through which the smoke traveled on its way to the stairwells. On the 12th floor, the ceiling was open to enable the rising smoke to be released. In each stairwell, a sensor (Almemo FVAD 35 TH4Kx, Ahlborn, Germany) was installed to measure the temperature and velocity of the rising smoke, as shown in Fig. 1b. The

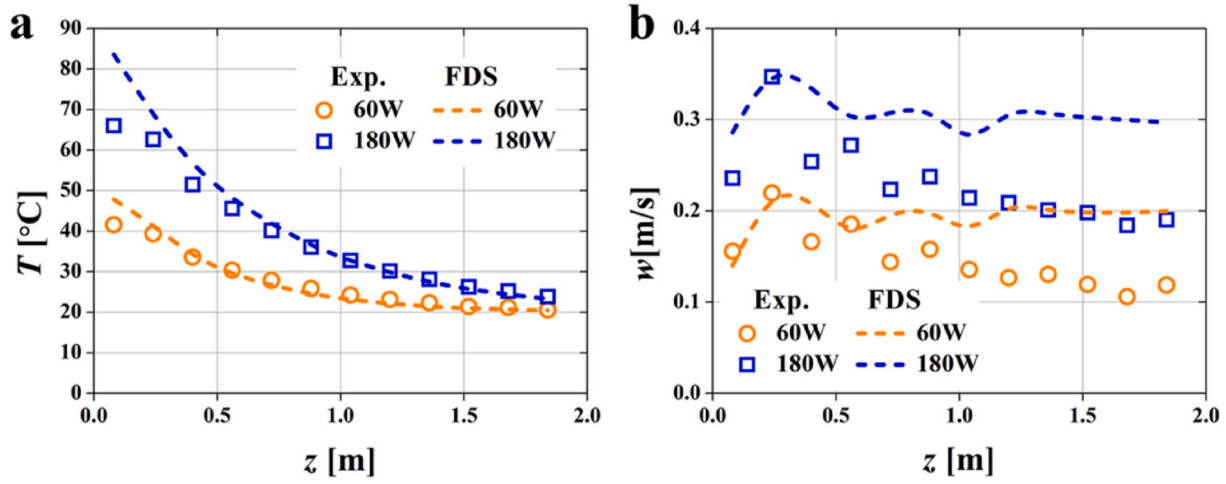

Fig. 4. Comparison between experimental data and FDS computational results for the smoke (a) temperature (T) and (b) velocity (w) at the steady state, in the case where all windows were closed.

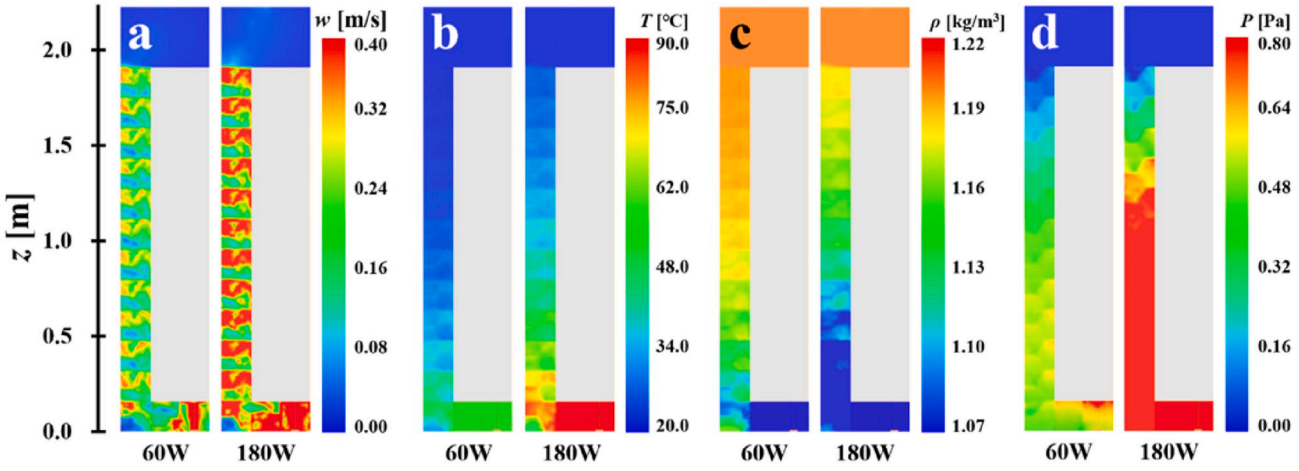

Fig. 5. Smoke characteristics in the case of $Q = 60$ W (left) and 180 W (right). The distributions of (a) w, velocity in the z-direction, (b) temperature T, (c) density ρ, and (d) pressure P in the vertical z-direction with all windows closed.

sensor head thickness was 6 mm, small enough not to interfere with the overall smoke flow pattern inside each floor having a height of 170 mm.

At the outer side of Room A, a window was located, as depicted in Fig. 1c, that was sealed with aluminum foil to prevent air leak or intake. This foil seal was removed when the window was open. The total length of each floor was 0.5 m including Rooms A and B and the stairwell; this distance was equally divided among the three compartments.

2.2. Uncertainty evaluation

Overall uncertainties, $(U_R)_{0.95}$, defined by Eq. (27) of Moffat [47] involving the temperature (T) and velocity (w) measurements have been estimated as:

$$(U_R)_{0.95} = \left\{(B_R)^2 + (tS_R)^2\right\}^{1/2} \quad (1)$$

Uncertainty guidelines suggested by Ref. [48] have been used to compute $(U_R)_{0.95}$. The sensor used (FVAD 35 TH4Kx) is capable of measuring velocity in the $0.08 \le w \le 2.0$ m/s range with the uncertainty level of $\sigma_w = \pm 0.04$ m/s and the resolution of $\Delta_w = 0.001$ m/s. The sensor had the temperature measurement range of $-20 \le T \le 70$ °C with the uncertainty level of $\sigma_T = \pm 0.7$ °C and the resolution of $\Delta_T = 0.1$ °C.

The bias limit of the sensor and its resolution is defined as B_{acr} and B_{rsl}, respectively, and the square root of the sum of their squared values is defined as B_R according to Eq. (25) in Moffat [47]:

$$B_R = \left\{(B_{acr})^2 + (B_{rsl})^2\right\}^{1/2} \quad (2)$$

Herein, the sensor accuracy has a normal distribution and the standard uncertainty, u_{acr}. It is found by dividing the half-range ($\sigma/2$) of the overall uncertainty (U_{acr}) by $k = 2$, which is known as the coverage factor according to Eq. (18) in Ref. [48]:

$$B_{acr} = U_{acr} = u_{acr}k = \frac{\sigma}{2}k \quad (3)$$

The uncertainty level of B_{acr} was found to be $B_{acr} = 0.04$ m/s for velocity and $B_{acr} = 0.7$ °C for temperature from the sensor specification, respectively.

The sensor resolution has a square distribution and its standard uncertainty, u_{rsl}, is related with the half-range (r=$\Delta/2$) of U_{rsl} according to Eq. (7) of Ref. [48]:

$$B_{rsl} = U_{rsl} = u_{rsl}k = \frac{r}{\sqrt{3}}k \quad (4)$$

The value of B_{rsl} from the sensor specification was 0.0006 m/s and 0.06 °C for w and T, respectively. As a result, the bias limit B_R is found to be 0.04 m/s for w and 0.7 °C for T according to Eq. (2).

Prior to all measurements, the heating power was supplied for 90 min to provide a steady-state flow of the surrounding air that ensures

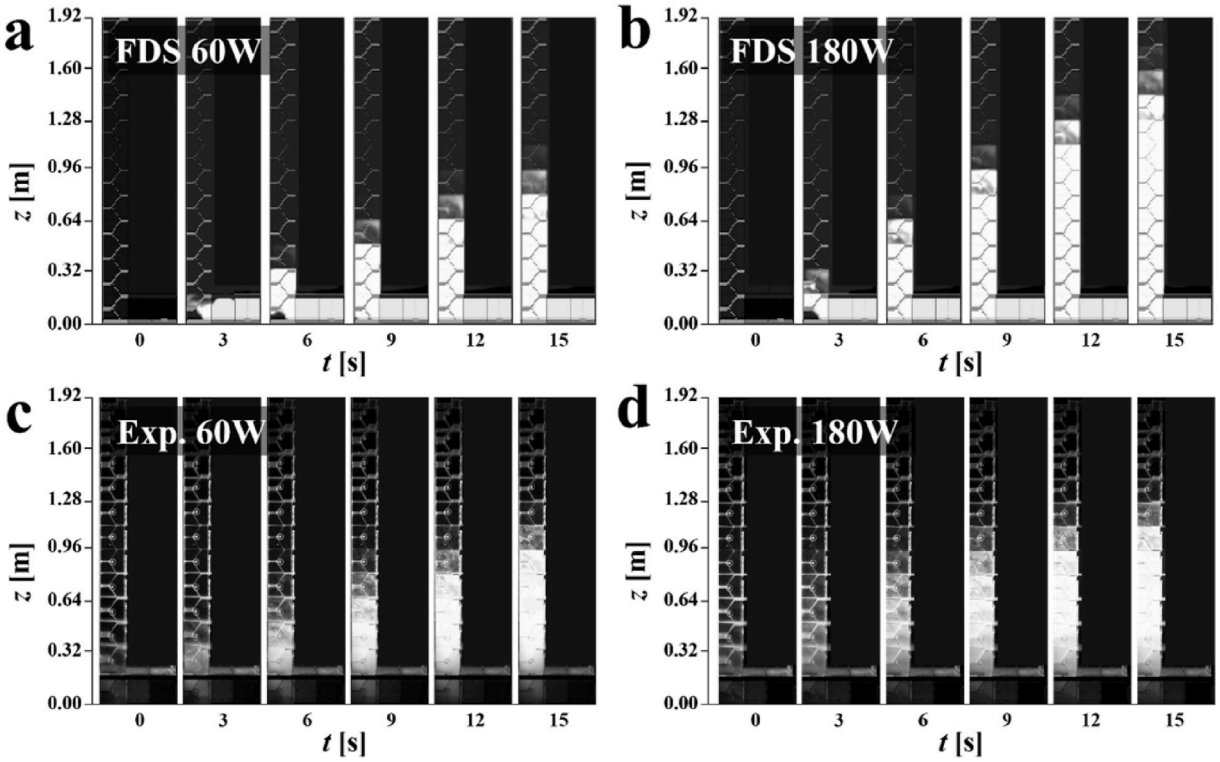

Fig. 6. Transient distribution of the rising smoke for: (a) FDS predictions at $Q = 60$ W, (b) FDS predictions at $Q = 180$ W, (c) the experiment at $Q = 60$ W, and (d) the experiment at $Q = 180$ W, with all windows closed in all cases.

supply of stable data for all sensors. After the flow was stabilized, measurement values were collected for every sensor at every measurement with the number of the measurements $N = 1800$.

In addition, N for each sensor was used to estimate the standard deviation S_R for every measurement. Equation (26) in Moffat [47] is used as follows:

$$S_R = \left\{ \sum_{i=1}^{N} \left(\frac{\partial R}{\partial X_i} S_i \right)^2 \right\}^{1/2} \tag{5}$$

The range of the standard deviation of each measurement for w and T is $0.002 \leq S_R \leq 0.038$ m/s and $0.02 \leq S_R \leq 0.88$ °C, respectively. Then, the multiplier factor $t = 1/\sqrt{N}$ is used to represent the uncertainty of measurement, u_S, based on Eq. (5) of Ref. [48]:

$$tS_R = U_S = u_S k = \frac{S_R}{\sqrt{N}} k \tag{6}$$

The range of U_S from Eq. (6) is $0.0002 \leq U_S \leq 0.0018$ m/s for w and $0.001 \leq U_S \leq 0.04$ °C for T. In conclusion, the overall uncertainty $(U_R)_{0.95}$ according to Eq. (1) is ±0.04 m/s for w and ±0.7 °C for T with the confidence level of 95%.

3. Modeling description

3.1. Fire Dynamics Simulator

To solve the Navier–Stokes equations for low-speed, thermally-driven smoke originating from fires, FDS software version 6.7.0 was used with a Mach number <0.3 [8–10,49–51]. The turbulence was modeled using the large eddy simulation (LES), and the combustion was modeled through mixture fraction analysis that presumed immediate reaction of fuel and oxygen. The radiation transport calculations were based on a non-scattering gray gas and a wide-band model. The radiation model was applied for large-scale fire (i.e., a few MW fires) while the radiation model was turned off for the small scale fires (i.e., under 1 kW). The governing equations that includ the continuity, species concentration balance, momentum and energy balances, and the ideal gas law [52], read, respectively,

$$\frac{\partial \rho}{\partial t} + \nabla \cdot (\rho \mathbf{u}) = 0, \tag{7}$$

$$\frac{\partial \rho Y_\alpha}{\partial t} + \nabla \cdot (\rho Y_\alpha \mathbf{u}) = \nabla \cdot (\rho D_\alpha \nabla Y_\alpha) + \dot{m}_\alpha, \tag{8}$$

$$\frac{\partial \rho \mathbf{u}}{\partial t} + \nabla \cdot (\rho \mathbf{u}\mathbf{u}) = -\nabla \tilde{p} - \nabla \cdot \tau + (\rho - \rho_0)\mathbf{g}, \tag{9}$$

$$\frac{\partial \rho h_s}{\partial t} + \nabla \cdot (\rho h_s \mathbf{u}) = \frac{\mathrm{D}\overline{p}}{\mathrm{D}t} + \dot{q} - \nabla \cdot \dot{\mathbf{q}}'', \tag{10}$$

$$\rho = \frac{\overline{p}\,\overline{W}}{RT}, \tag{11}$$

where D_α is the turbulent diffusion coefficient of species α, $\mathbf{g}$ is the gravity acceleration, h_s is the mass-weighted average enthalpy of the lumped species [49], $\dot{m}_\alpha$ is the mass-production rate per unit volume of species α by chemical reaction, $\tilde{p}$ is the pressure perturbation, $\dot{q}$ is the heat release rate per unit volume, $\dot{\mathbf{q}}''$ is the heat flux vector, R is the universal gas constant, t is time, $\mathbf{u}$ is the velocity vector, $\overline{W}$ is the molecular weight of the gas mixture, and Y_α is the mass fraction of species α. The adiabatic no-slip wall boundary conditions were imposed at the bottom surface, and an open freestream boundary conditions were used for the remaining outer surfaces. The initial temperature was $T_\infty = 20$ °C.

3.2. Grid convergence studies

A grid-convergence study was carried out for the heat flux with $Q =$ 60 and 180 W with the vertical velocity 0.87 m/s at the first floor of stairwell domain (0.5 m × 0.15 m × 0.17 m) with the heat source size of

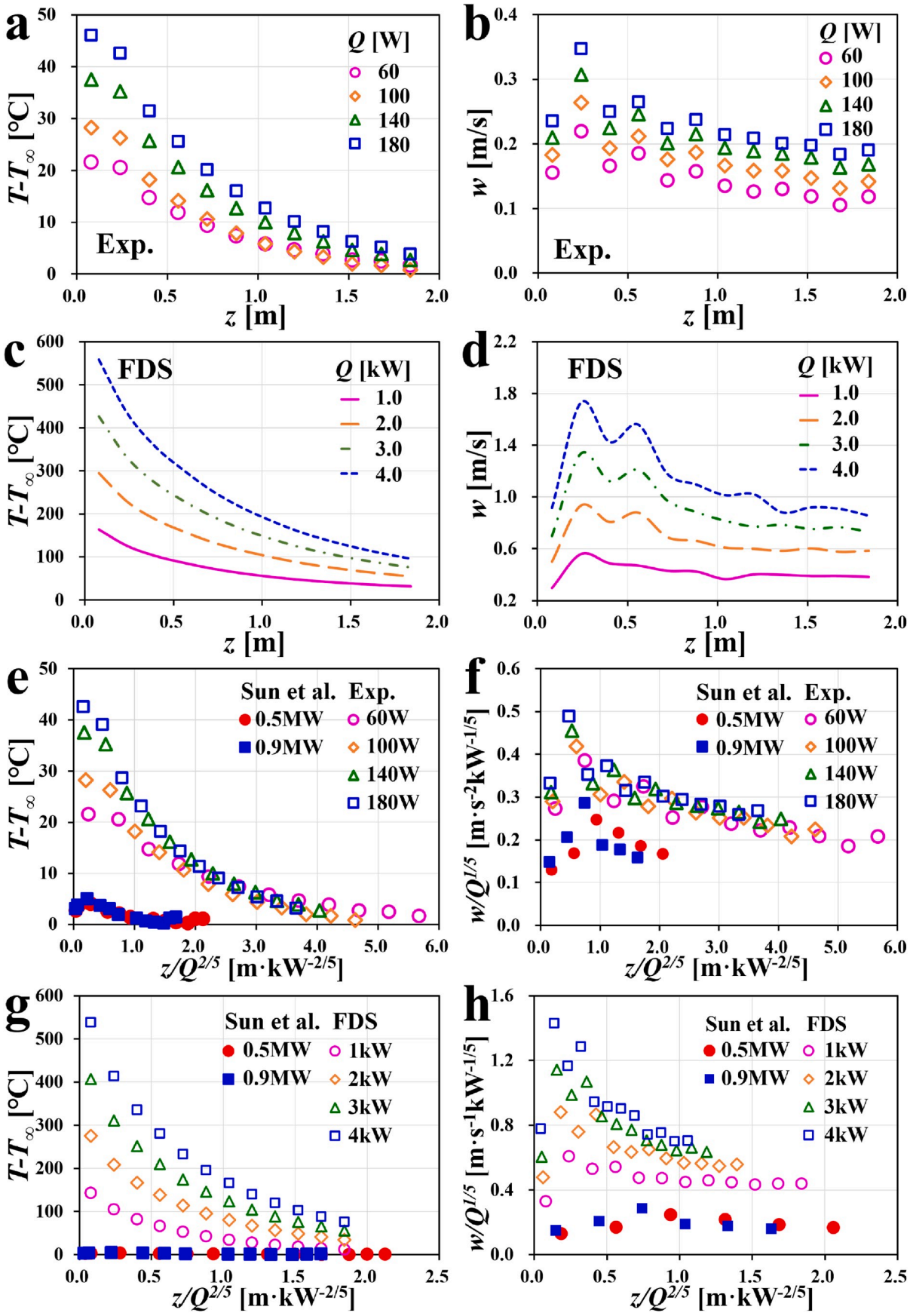

Fig. 7. Effect of heating power (or fire size) Q on (a) the experimentally measured temperature T and (b) velocity w and the numerical ones (c) T and (d) w. (e) The scaled experimental w and (f) the scaled numerical w are compared with the data of Sun et al. [34]. All windows are closed.

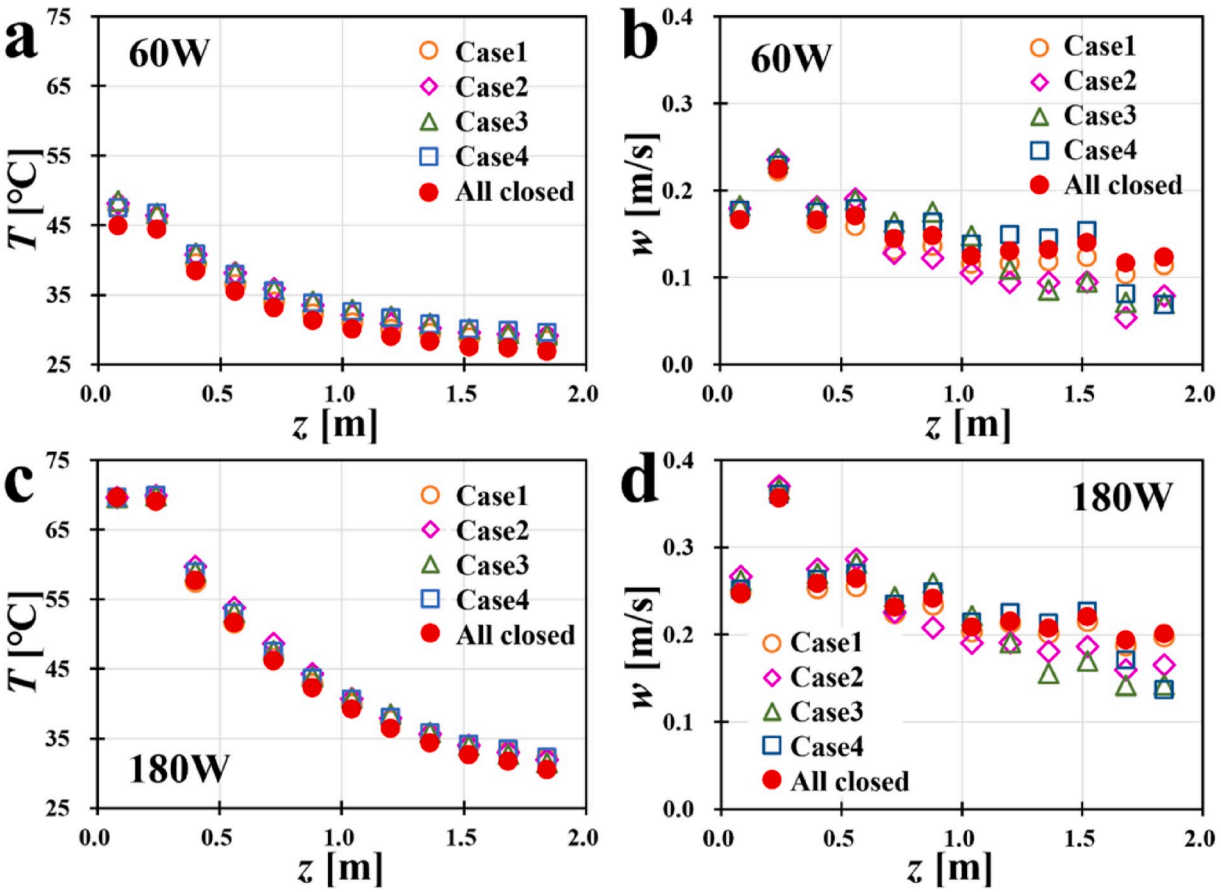

Fig. 8. Effect of open windows at various elevations for Cases 1, 2, 3, and 4. The rising smoke measurements include (a) T at $Q = 60$ W, (b) w at $Q = 60$ W, (c) T at $Q = 180$ W, and (d) w at $Q = 180$ W. Under these conditions, only one window was open.

0.0016 m^2 and the heating power of $Q = 60$ and 180 W for the first floor of the prototype building shown in Fig. 1. Grid resolutions of 24 × 11 × 8 (2,112 nodes), 47 × 22 × 16 (16,544 nodes), 94 × 43 × 32 (129,344 nodes), and 188 × 86 × 64 (1,034,752 nodes) were adopted as coarse, medium, medium-fine, and fine cases, respectively. It should be emphasized that FDS is a sub-grid scale (SGS) model that addresses important small-scale thermo-physical phenomena without resolving the small scale grid resolution. Physical and statistical models are implemented to address the small-scale flow physics, such as small eddies, swirls, and vortices [53–57].

Fig. 2 indicates that the medium-fine grid resolution was sufficient to resolve both temperature (T) and rising velocity (w) accurately for both $Q = 60$ and 180 W, which has yielded the grid spacing of $\Delta x = 0.0053$, $\Delta y = 0.0035$, and $\Delta z = 0.0053$. All data were acquired at the center of stairwell at $z = 0.17$ m. The bottom surface of the domain was specified as a no-flux (except at the heat source), perfectly insulated wall with no-slip conditions. Only upside of stairwell was opened for air to exit through all the walls. The initial air temperature and pressure were fixed at $T_\infty = 20$ °C and $P_\infty = 1$ bar, respectively. Simulations up to $t = 900$ s produced the grid-converged solutions between the medium-fine and fine resolutions.

3.3. Computational details for small-scale fires

In this study, "small-scale fire" refers to that in the prototype building shown in Fig. 1, with the dimensions of 0.5 m × 0.15 m × 2.0 m. Because the prototype is a 12-story building, the height of each floor was approximately 0.17 m. The length of Room A, Room B, and the stairwell was each 0.17 m; the width of the entire structure was 0.15 m. The total number of computational nodes used for this geometry was 94 × 43 × 384, which is about 1.55 × 10^6 nodes. Rectangular meshes with uniform interspace distance were used for all computations. No-slip boundary conditions were used for all walls, which were similar to the actual acrylic material. As a result, any possible heat loss through the acrylic wall was considered, just as that in actual cases. The radiation effect was neglected for small-scale fires with $Q < 1$ kW. All computations were conducted up to $t = 3600$ s, and the steady state was reached at $t = 3000$ s.

3.4. Computational details for large-scale fires

The numerical simulations were extended to large-scale fires once the FDS results were validated for the small-scale sets of experiments. Large-scale fire simulations are more realistic because the fire power is in the $2 \le Q \le 20$ MW range, and the building height reaches up to 120 m with 30 floors. Two sets of numerical simulations were conducted. The first included a 15-story building, 60 m in height with exact dimensions of 2.8 m × 10.0 m × 60 m, and the second included a 30-story building, 120 m in height with exact dimensions of 2.8 m × 10.0 m × 120 m. For these, the total number of computational nodes was 28 × 100 × 600 (1.68 M nodes) and 28 × 100 × 1200 (3.36 M nodes), respectively. The length of each floor was 10 m, which was divided into a 3-m corridor with a window, shown as the room at the far left of Fig. 3; a middle room of 1.5 m; and a stairwell of 5.5 m shown at the far right in the figure. All stairwells were connected in a spiral structure through which the smoke ascended. The dimensions of the open area of each stairwell was 4.1 m × 2.8 m, and all windows and doors were equal in size of 1 m × 2 m. Two air inlet sources were installed for all floors; one is the open stairwell through which smoke travels in a spiral pattern and the other is the window installed at the very end of the hallway, as

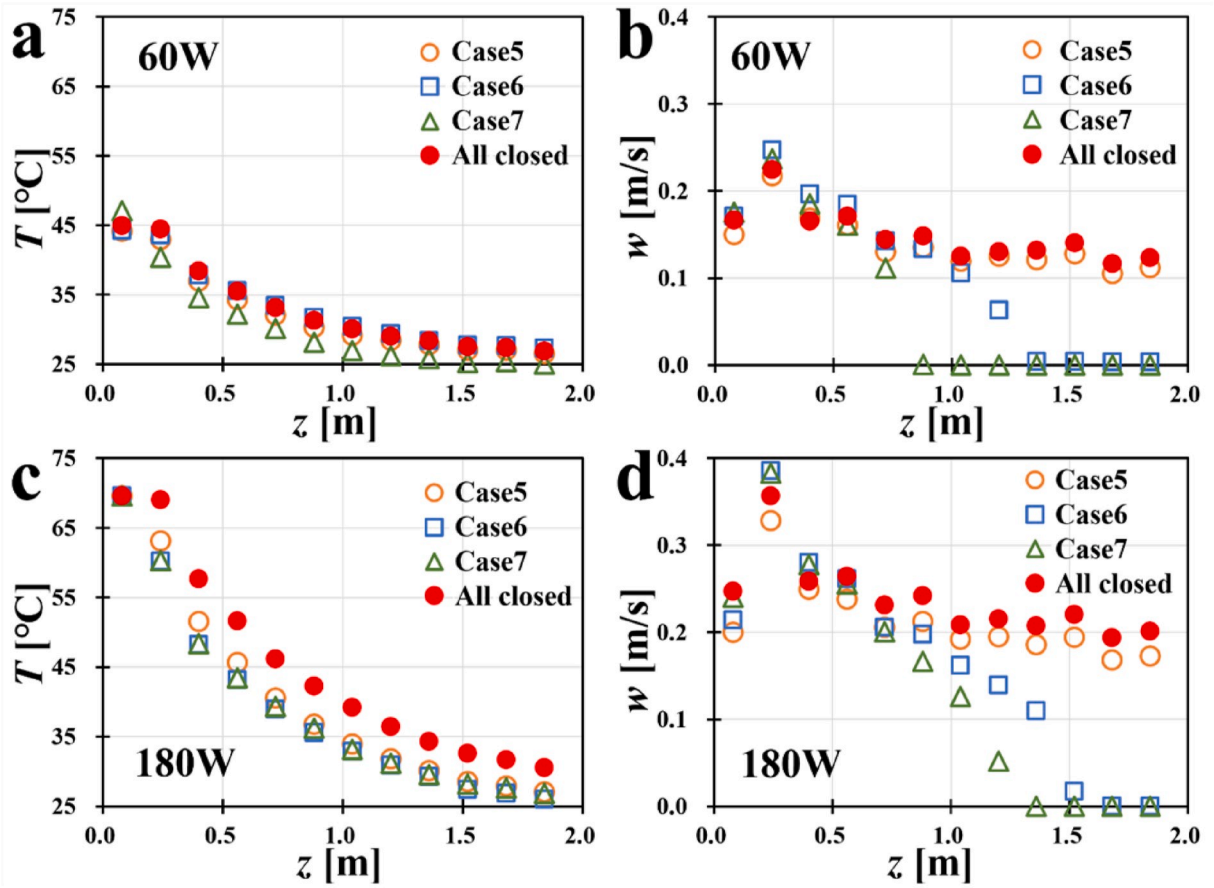

Fig. 9. Effect of open windows at various elevations for Cases 5, 6, and 7. The rising smoke measurements include (a) T at $Q = 60$ W, (b) w at $Q = 60$ W, (c) T at $Q = 180$ W, and (d) w at $Q = 180$ W. Under these conditions, only one window was open.

illustrated in Fig. 3a.

The fire size, or heating power, ranged from 2 to 20 MW; octane was used as the fuel. Rectangular meshes of uniform interspace distance were used for all computations. No-slip boundary conditions were used for all walls, which were treated as actual concrete. As a result, any possible heat losses through the concrete wall were accounted for, just as that in actual cases. The radiation transport calculations based on a non-scattering gray gas and a wide-band model were used for large-scale fires (i.e., a few MW fires). The concrete wall thickness was 0.2 m, and the thermal conductivity, specific heat, and density values were 1.7 W/m·K, 0.9 kJ/kg·K, and 2300 kg/m^3, respectively. The surrounding air temperature was set at 20 °C. All computations were conducted up to $t =$ 7200 s, and the steady-state was reached at $t = 5400$ s, beyond which the fires were assumed to be fully developed. The growing/developing or t^2 fire growth curves [58] were not considered for data acquisition.

4. Results and discussion

4.1. Experiment and modeling for all-windows-closed case

Fig. 4 compares the experimental data and FDS results for the rising smoke temperature and velocity at the steady state. All building windows were closed, and the ceiling at the top floor was the only outlet for the smoke, as depicted in Fig. 1a. Both the temperature (T) and vertical velocity (w) decreased with an increase in the vertical elevation (z), as measured by the installed sensors shown in Fig. 1b. The range of w is moderately low, which corresponds to the moderate fire heating power of $Q = 60$ and 180 W, especially when the flow is confined in a reduced-scale building prototype. In a large-scale with a few MW-power fires, the rising velocity of the smoke away from the building wall is in the range of a few m/s. Both experimental and FDS simulation data provide the rising velocity less than 1 m/s. The FDS results tend to over-predict the rising velocity for both $Q = 60$ and 180 W because the FDS model underestimates the significance of the wall boundary layer during a very slow flow such as $w < 1$ m/s. Both the T and w values were highest at the locations closest to the heat source ($z \rightarrow 0$); both thermal energy and momentum dissipated along the building height. When the fire power increased from $Q = 60$ W to 180 W, both the T and w values increased. Fig. 4a shows that FDS prediction agreed well with the experimental data, and Fig. 4b shows that the FDS predicted a sudden increase in vertical velocity at $z = 0.25$ m. The smoke motion was steady and slow from the heat source and across the hallway on the first floor. However, the smoke motion accelerated when the smoke reached the stairwell. This was expected because the stairwell was designed to create suction owing to the stack effect, which exists only in the vertical direction because of the buoyancy force. This stack effect, or chimney effect, explains the sudden increase in the smoke velocity shown in Fig. 4b. Then, the smoke motion slowed, while traveling through the building because of momentum dissipation at the walls and stairs, even though the velocity did not reach zero at the building top ($z = 2$ m). FDS tended to over-predict the smoke velocity, with the prediction deviating from the experimental data in the upper locations of the building ($z \geq 0.5$ m). In experiments, the smoke flow was turbulent even at this low heating power of $Q = 60$ W, and the complexities were magnified by obstructions in the spiral stairwells. When all windows were closed, the air-suction effect through the stairwell was over-predicted by FDS. This deviation can be attributed to the pressure boundary condition at the inlet and outlet, which enhanced the pressure drop ΔP.

Fig. 5 compares the fields of velocity, temperature, density, and pressure in the rising smoke in the stairwells at various vertical

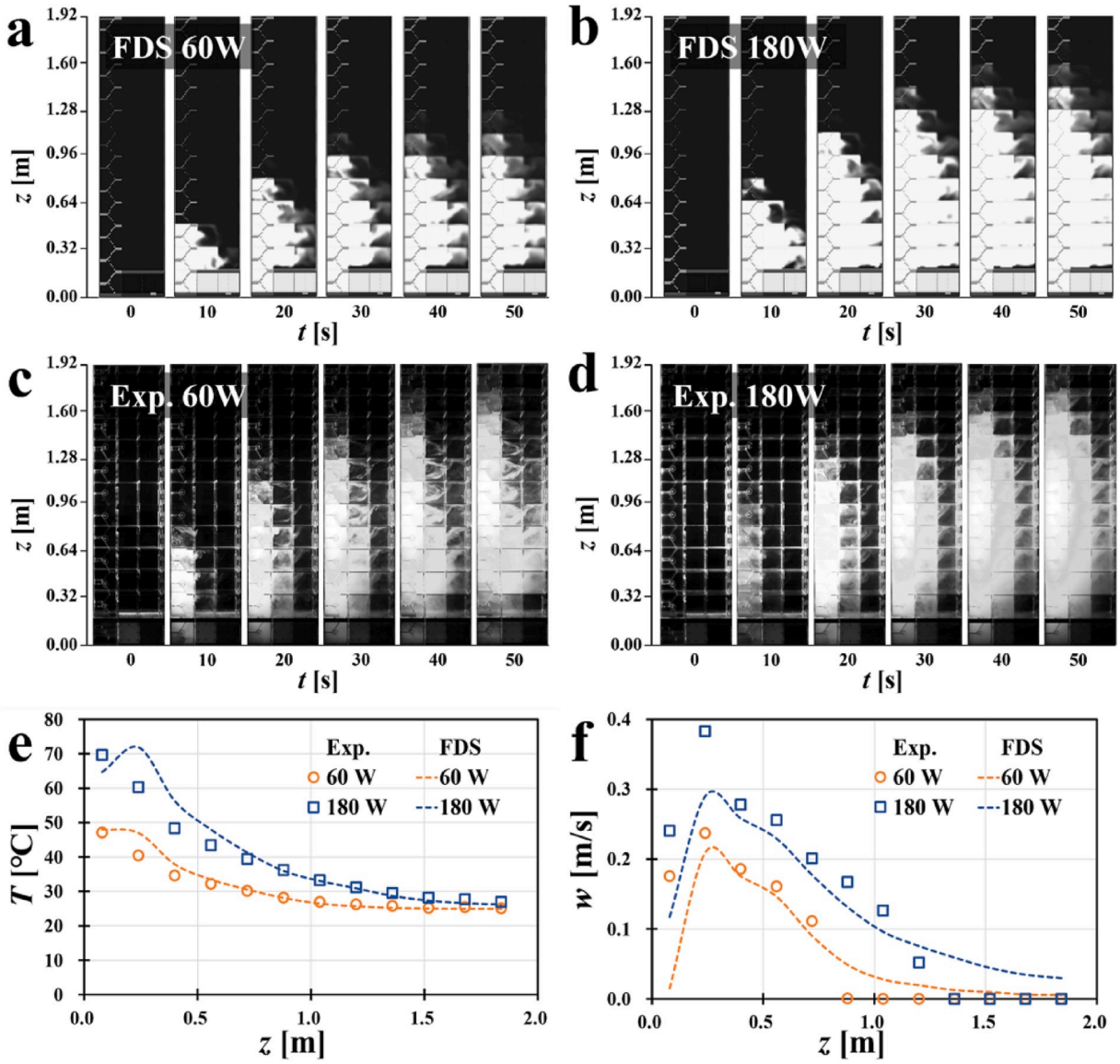

Fig. 10. Transient distribution of the rising smoke for (a) the FDS predictions at $Q = 60$ W, (b) the FDS predictions at $Q = 180$ W, (c) the experiment at $Q = 60$ W, and (d) the experiment at $Q = 180$ W when all windows were open. Also shown is a comparison between the experimental data and the FDS results for smoke: (e) temperature (T) and (f) velocity (w) in the steady state with all windows open.

elevations for $Q = 60$ W (left) and 180 W (right). Fig. 5a shows that a higher velocity w results from a more powerful fire (a higher Q). The velocity alternated while the smoke flowed through the spiral stairwell structure in the vertical direction. In Fig. 5b, a higher temperature T also results from a more powerful fire (a higher Q). A temperature reduction with the ascent of smoke in the spiral stairwells is clearly visible. In Fig. 5c, the smoke density is shown to increase toward the top of the building. The rising smoke cools, which increases its density, and the heat dissipates through the surrounding walls. It is noted that accumulation of smoke products such as soot cannot be the reason for the density increase at higher locations because soot was not modeled during simulations. The pressure distribution is shown in Fig. 5d. However, because the pressure difference between the top and bottom positions remained less than $\Delta P = 1$ Pa, whose effect is quite insignificant. The increase in pressure at the bottom is attributed to hot air expansion in a confined area. A typical stack pressure distribution, with low values at the bottom and high values at the top, would have resulted if the stairwells had mimicked a typical shaft flow with reasonably strong buoyancy or fire size. As follows from Fig. 5, the buoyancy force was moderate in the present case, thus, a strong stack effect was not observed.

Fig. 6 compares the images of the rising smoke obtained during the experiments in comparison with those from the FDS simulations. The smoke reached the top of the building within $t = 15$ s for the experiments and the FDS simulations. Thus, the results are in good agreement qualitatively. When the fire power was greater ($Q = 180$ W), the smoke reached the top faster because a stronger buoyancy force was presented. As shown in Fig. 4b, FDS slightly overpredicted the rate of smoke rise, which is consistent with what was qualitatively presented in Fig. 6.

4.2. Experiment and modeling of the effect of fire power Q with all windows closed

The modeling results were validated against the experimental data given in the previous section 4.1 for the case with all windows closed. In the present section, the effect of heating power (Q) on T and w is investigated. The range of the heating power was 60 W $\leq Q \leq$ 180 W for the experiments and 1 kW $\leq Q \leq$ 4 kW for the FDS simulations, the latter was done to extrapolate the results to real buildings. An experiment for Q beyond 180 W was impossible because of melting of the acrylic

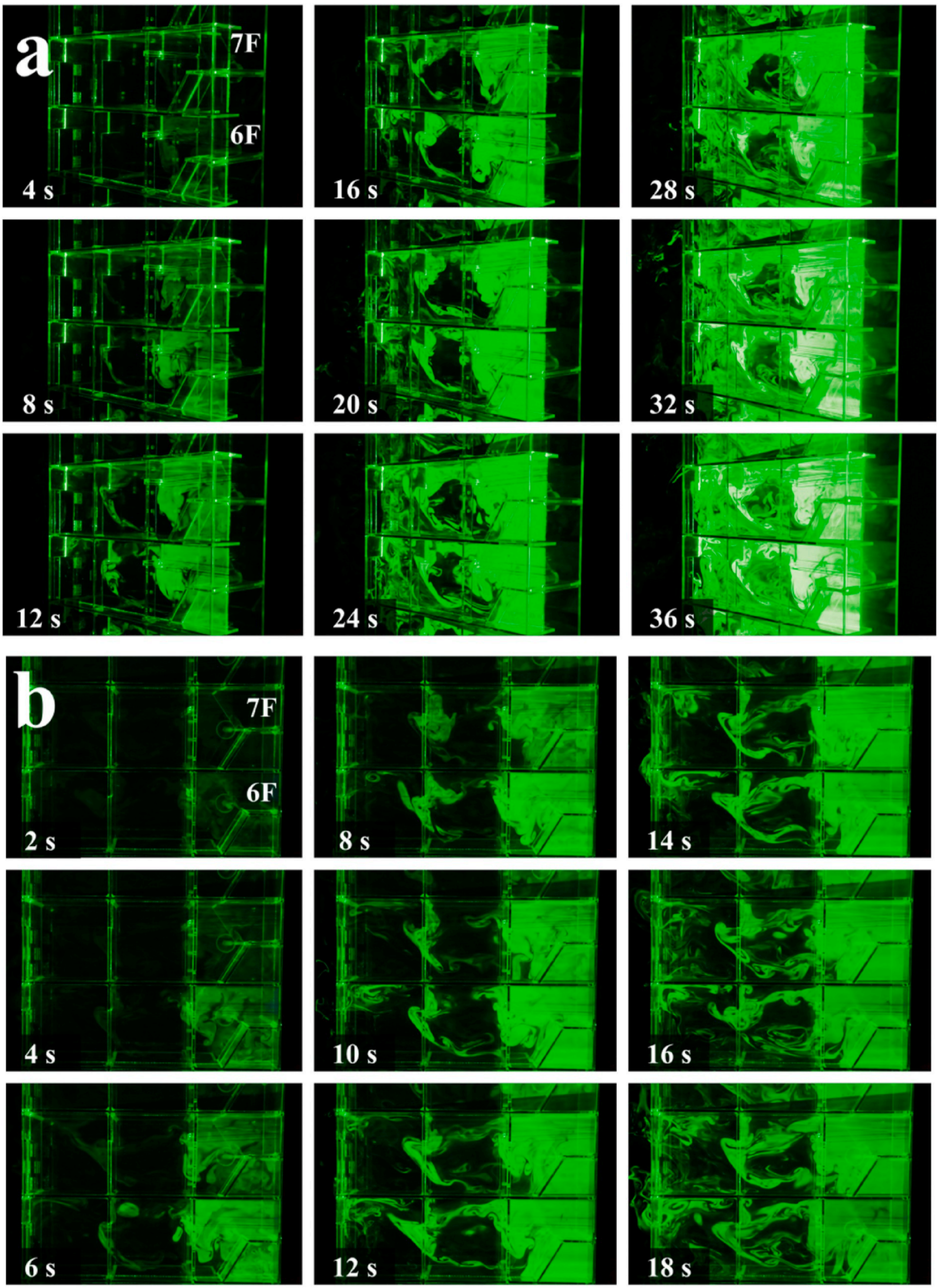

Fig. 11. Time series images of the rising smoke inside a transparent building with stairwells in Case 7: (a) angle view; (b) side view.

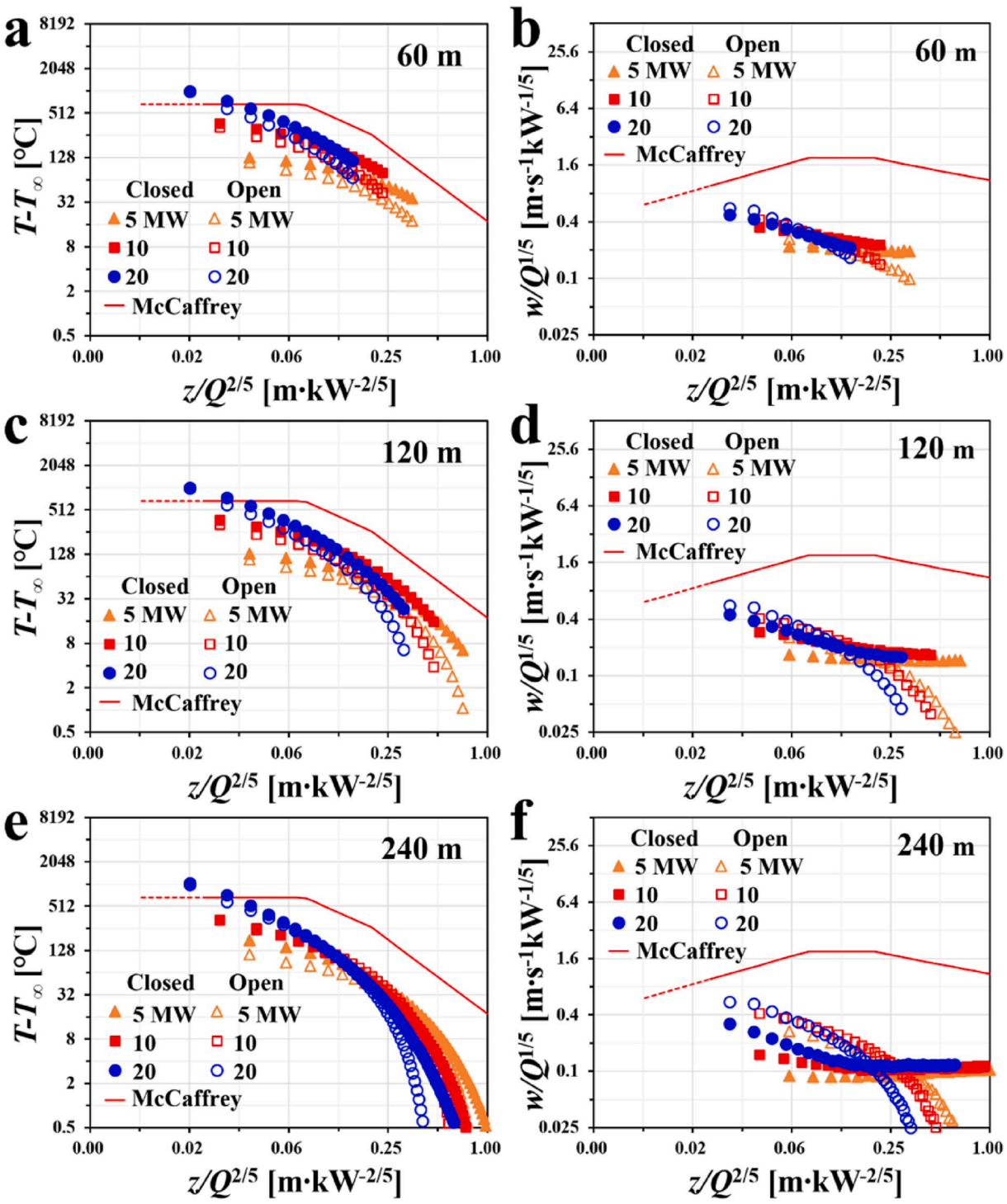

Fig. 12. Temperature (T) and velocity (w) distribution along the log-scale z-direction for large-scale fires inside buildings of 60 m, 120 m, and 240 m in height. (a) T and (b) w inside the 60-m building, (c) T and (d) w inside the 120-m building, (e) T and (d) w inside the 240-m building. Both w and z were scaled by $Q^{1/2}$ and $Q^{2/5}$, respectively, for data collapse onto master curves. These computational FDS results were compared with the empirical data for the open-air plume by McCaffrey [12].

material.

Fig. 7 shows that both T and w decreased with distance from the heat source at $z = 0$ m, with both the thermal energy removed through the walls and momentum dissipating in the vertical direction. In addition, a larger fire power Q induced a higher temperature T and velocity w for both experiment and the FDS predictions, as shown in Fig. 7a–d. When z was scaled with $Q^{2/5}$, the results for both T and w could be collapsed on a single master curve; see Fig. 7e and f, which includes the experimental data of Sun et al. [34]. In the experiment of [34], the stairwell column (or shaft) was completely confined except for the bottom first floor inlet and the top sixth floor outlet. Thus, the building structure of Sun et al. [34] was very similar to the present scenario under the all-windows-closed conditions. Therefore, a comparison between the data of Sun et al. [34] and the present simulations is relevant.

The sudden increase in velocity w near the heat source is explained by the initial suction of the smoke at the first floor stairwell, followed by a decrease in w with distance from the heat source. It is interesting to note that Sun et al. [34] observed a similar trend, even though their fire

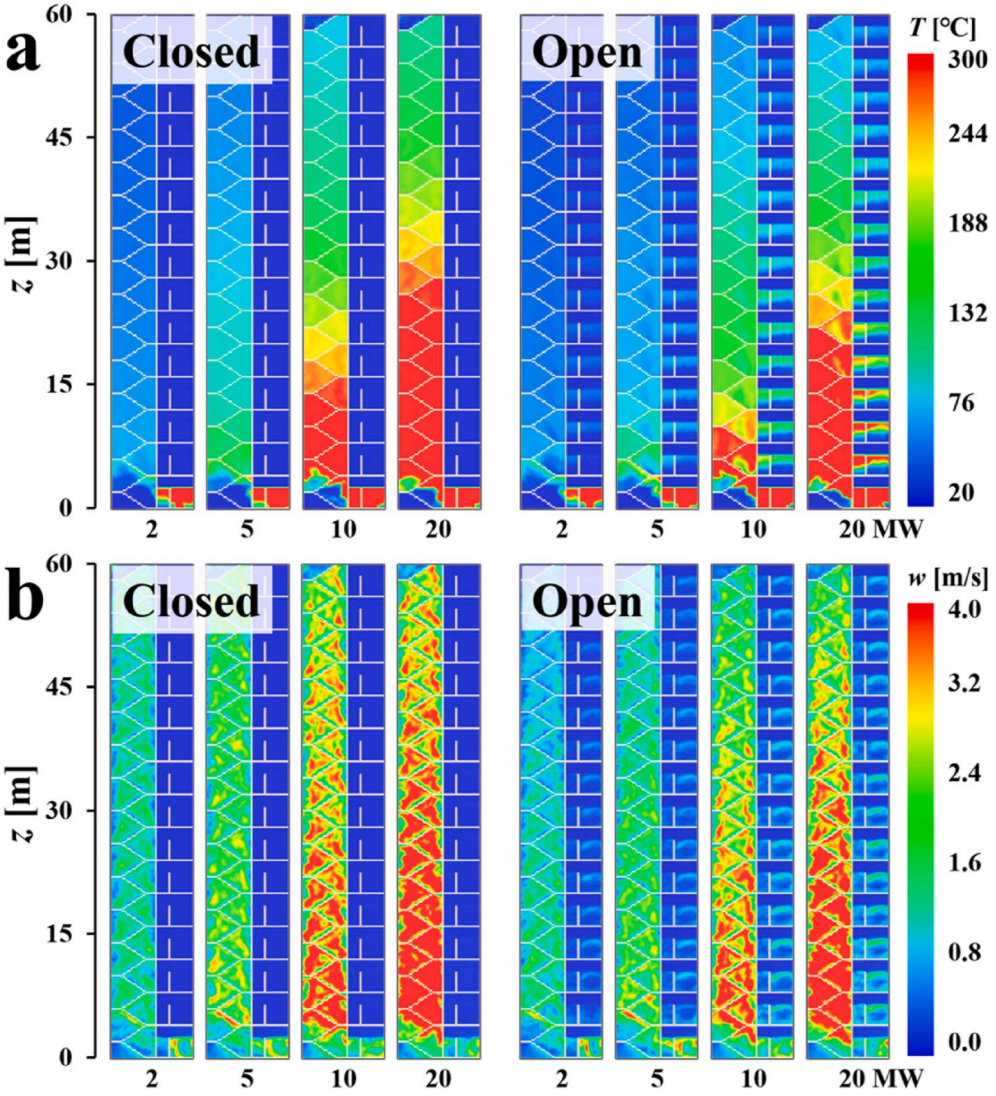

Fig. 13. Time-averaged steady-state temperature (T) and velocity (w) distributions in the rising smoke inside the 60-m-tall building with varying fire power Q from 2 to 20 MW with the all-closed windows (left) and all-open (right) windows.

size was on a much larger scale ($0.5 \leq Q \leq 0.9$ MW). This initial air suction effect was fully revealed in the FDS simulations, as shown in Fig. 7d and h. In Fig. 7g–7h, the effect of Q is also apparent, even though w is scaled by $Q^{2/5}$, indicating that FDS captured this initial air suction phenomenon quite accurately. When the data of Sun et al. [34] were plotted using the same scale as that of the FDS results, the air suction effect appeared to be nonexistent for T and moderate for w, as shown in Fig. 7g and h, respectively. Although this suction effect is authentic, it could be difficult to capture in a very large-scale fire with sparse data. It should be emphasized that a moderate flow speed ($\leq$1 m/s) had minor effect on the temperature, particularly on a temperature scale of 10^2 °C (Fig. 7g).

4.3. Experiment for the effect of open windows

The effect of the number of open windows (or opening ratio) on flow characteristics has been addressed in this section. In Fig. 8, only one window was opened at different floors, while in Fig. 9, the case of the greater number of open windows was explored and compared with the all-windows closed case.

Fig. 8 compares the experimentally measured temperature and velocity of the rising smoke for different open-window scenarios. Cases 1, 2, 3, and 4 refer to one window open at the second, fifth, eighth, and eleventh floors, respectively. The smoke temperature (T) and velocity (w) in Cases 1, 2, 3, and 4 are compared with their counterparts in the all-windows-closed case shown in Fig. 4. As can be seen from this comparison, both T and w in the one-window-open cases did not deviate substantially from the values in the all-windows-closed case. Thus, it is safe to conclude that one open window does not alter the overall patterns of both T and w regardless of the open-window location. The effect of the intake fresh air by one window was insignificant for the overall flow characteristics. This trend was consistent regardless of the fire power Q.

Fig. 9 compares the temperature and velocity of the rising smoke for different open-window scenarios. Case 5 refers to five open windows at the second, third, fourth, fifth, and sixth floors. Case 6 refers to six open windows at the seventh, eighth, ninth, tenth, eleventh, and twelfth floors. Case 7 refers to all windows open except for the one at the first floor. These cases were compared with the all-windows-closed case shown in Fig. 4. Opening five, six, or eleven windows caused a temperature drop, as shown in Fig. 9a and c. The temperature drop was largest for Case 7, which had eleven open windows, because a greater volume of fresh, cool air was taken in. Similarly, the velocity decreased substantially for these open-window cases. As shown in Fig. 9b and d, the velocity drop was also greatest for Case 7, owing to the large volume of fresh air taken in through the eleven open windows. This air intake

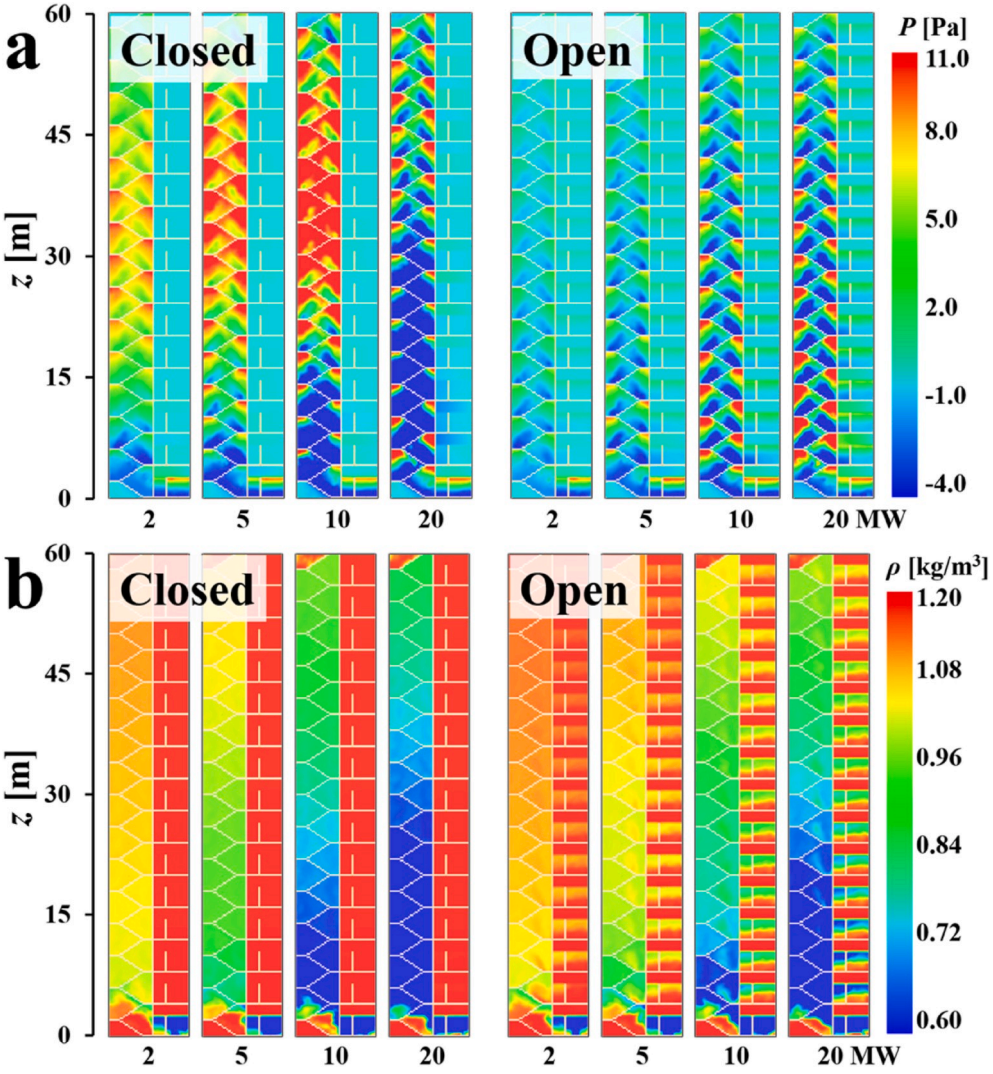

Fig. 14. Time-averaged steady-state pressure (P) and density (ρ) distributions in the rising smoke inside the 60-m building with varying Q from 2 to 20 MW in the all-windows-closed (left) and all-windows-open (right) cases.

decelerated the buoyancy-driven smoke rise and eventually stopped the air flow. For the fire power of $Q = 60$ W and $Q = 180$ W, the flow was completely stopped and became stagnant beyond at $z \geq 0.75$ m and $z \geq 1.3$ m, respectively. It is noteworthy that for Case 5, the velocity reduction was nearly zero, as compared with the all-window-closed case (Fig. 9b and d). This result indicates that the air suction at the lower floors was insignificant; most of the air intake originated from the upper floor, which eventually slowed the smoke motion. This is demonstrated in Case 6. It should also be emphasized that the overall velocity shown in Fig. 9d is greater than that in Fig. 9b because of the greater Q.

In summary, when the number of open windows exceeds five, the location of the open windows had a significant impact on w. The overall temperature T reduced with opening windows, but the location of the open-windows had no effect on T. The chimney or stack effect has not been simulated because the temperature and pressure difference between the building inside and outside is insignificant. The outside temperature was set to $T_\infty = 20$ °C, and thus, the stack effect was minimized with relatively small temperature difference between inside and outside the building. The pressure difference between inside and outside remained well below $\Delta P < 10$ Pa, which is too small to drive a visible stack effect in the entire building and thus the NPP (neutral plane position) is essentially non-existent.

4.4. Experiment and modeling for the all-windows-open case

Fig. 10 compares the smoke rise images obtained during the experiment and predicted using the FDS simulations for both $Q = 60$ W and 180 W, with all windows open. The qualitative and quantitative comparisons are shown in Fig. 10a–d and Fig. 10e and f for temperature T and velocity w, respectively. Both the temperature T and velocity w profiles revealed an excellent agreement between the experimental data and the FDS predictions in the present all-windows-open case. A sufficient supply of air through the open windows quickly diminished temperatre T and velocity w in the z-direction, which is different from Fig. 4 for the all-windows-closed case. When all windows were closed, the flow inside the stairwells exhibited the characteristics of a shaft flow, which facilitates constant axial velocity. However, as shown in Fig. 10 for the all-windows-open case, the flow more closely resembled a classical plume flow under open-air condition. Thus, the plume quickly weakened because of the entrainment of the surrounding air and reached stagnation. This plume weakening was very effectively predicted using the FDS simulations, with the results being in good agreement with the experimental data. Therefore, the accuracy of both the computations and experiments is cross-corroborated.

Fig. 11 shows time series images of rising smoke inside a building prototype at the sixth and seventh floors. Fig. 11a and b shows the angle

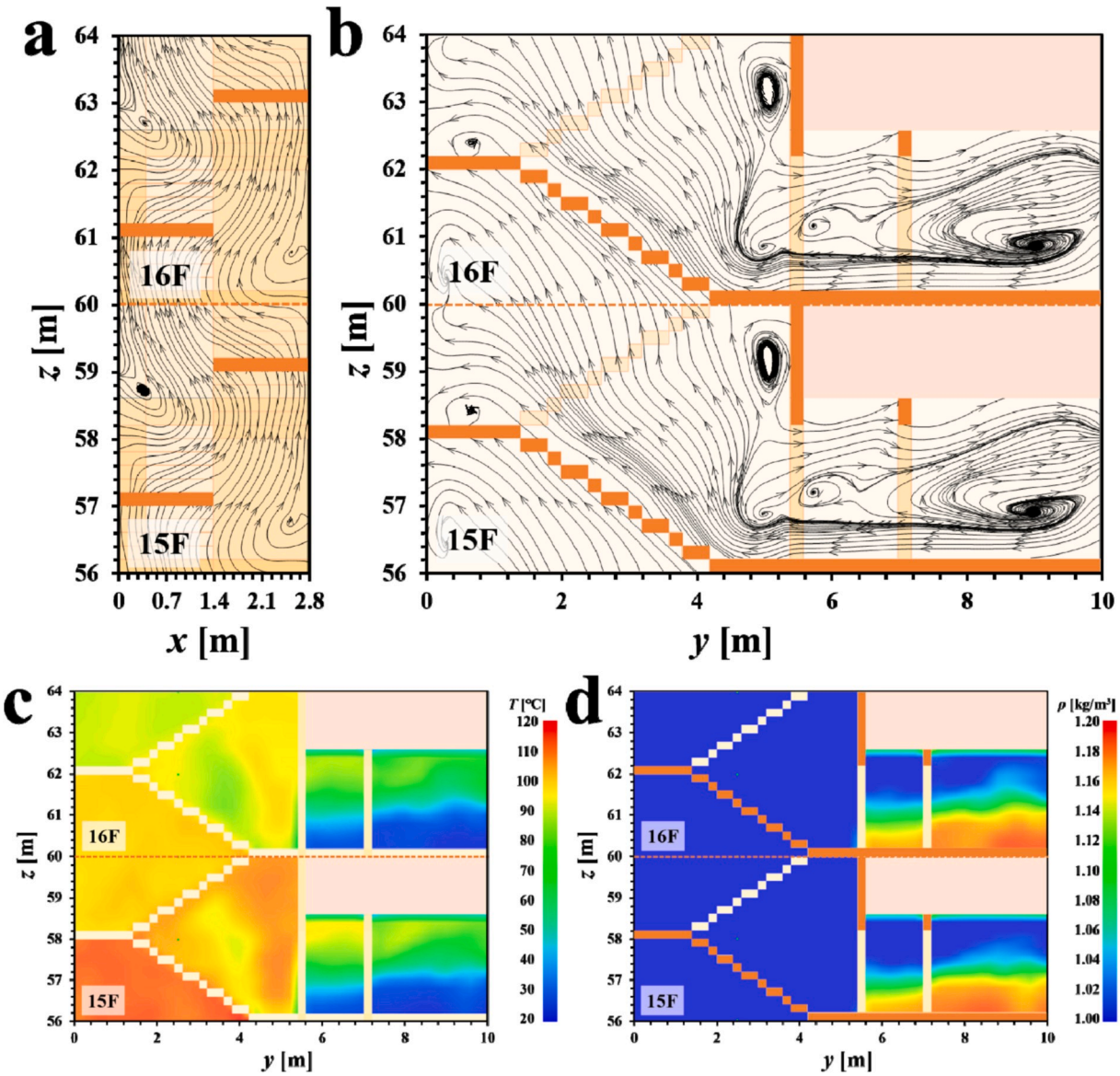

Fig. 15. Cross-sectional view of the 120-m building at the 15th and 16th floors, depicting the streamlines of smoke flow inside the corridor, middle room, and stairwells.

and side views of the building with rising smoke inside. Movies S1, S2, and S3 show the complexities involved in the smoke flow inside this building. Movie S1 shows the front view of the building width, in which the smoke rotates in the spanwise direction on every floor while moving upward. Thus, this flow pattern differs significantly from the classical plume arising under open-air conditions. Movie S2, which includes images from Fig. 11a, shows that the rising smoke traveled along the ceiling on every floor and entirely filled Rooms A and B. The smoke traveled along the ceiling and rotated inside each room. Then, it infiltrated the next room, and this vortical flow pattern was repeated. Upon contact with the window, the smoke escaped outside. At the same time, fresh, cool air was drawn into the rooms and diluted the smoke, which eventually resulted in decrease in the smoke temperature and velocity. These videos for the first time provide an insight into the smoke flow inside a building equipped with stairwells.

Supplementary video related to this article can be found at https://doi.org/10.1016/j.ijthermalsci.2020.106500

Supplementary video related to this article can be found at https://doi.org/10.1016/j.ijthermalsci.2020.106500

Supplementary video related to this article can be found at https://doi.org/10.1016/j.ijthermalsci.2020.106500

4.5. Modeling of the large-scale fires

The numerical simulations were extended to larger-scale fires with heating power in the $2 \leq Q \leq 20$ MW range. Fig. 12 compares these numerical results for the large-scale fire inside a building with the empirical data of McCaffrey [12], which is available for only the classical plume under open-air conditions. This comparison quantitatively shows various deviations of the building smoke characteristics, as compared to the open-air plume data of McCaffrey [12]. The results for buildings of $H = 60$, 120, and 240 m in height deviated significantly from the empirical fits of McCaffrey [12]. This result was expected because the smoke dynamics are inherently different under open-air conditions from those inside buildings, in particular, when the building geometry is complex and includes stairwells, hallways, and windows. As shown in Fig. 12, for most locations in the z-direction, both temperature T and velocity w were lower when the building windows were open because the intake of fresh air slowed down and cooled the smoke. These numerical patterns did not differ significantly from those

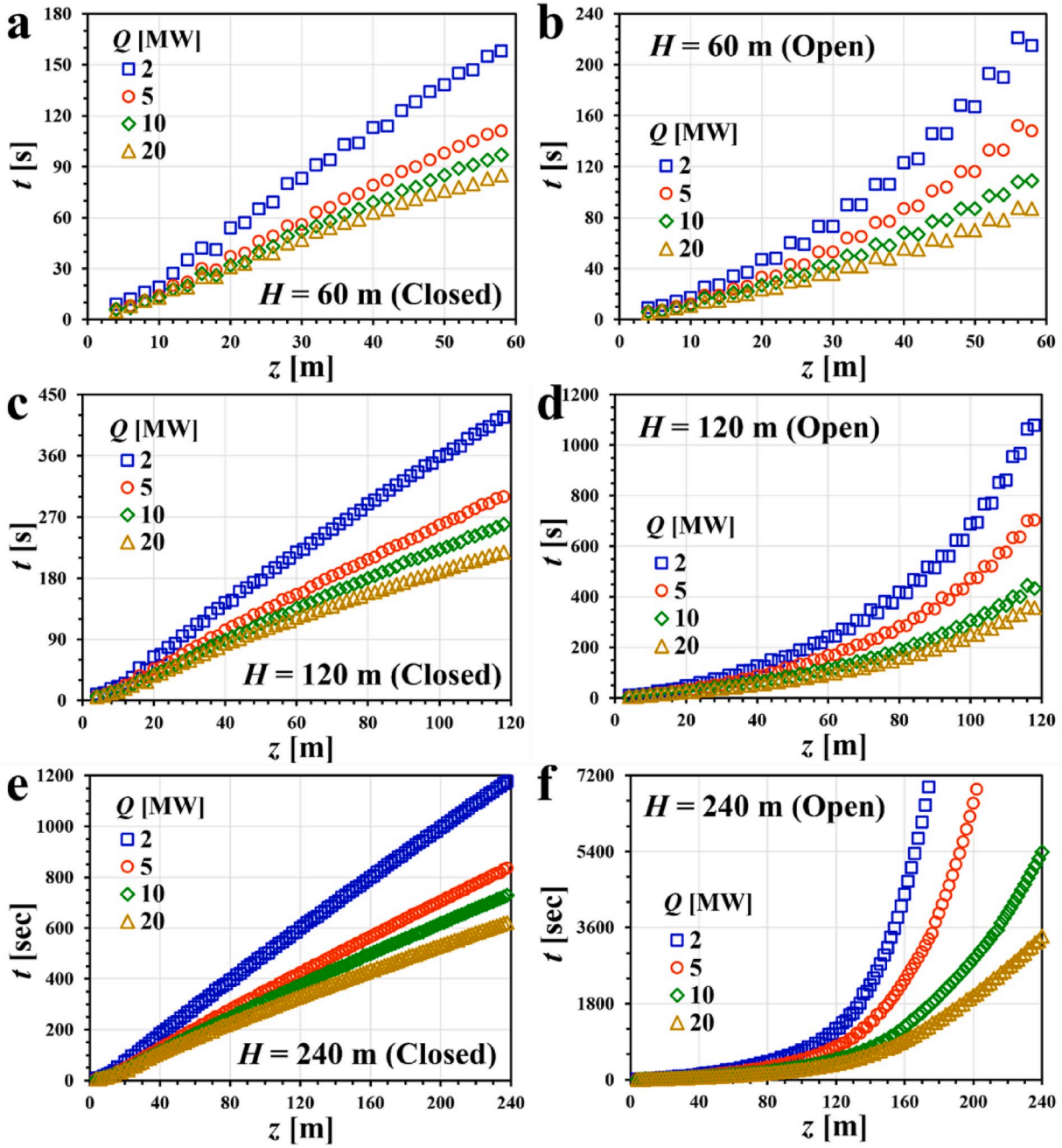

Fig. 16. Smoke rising time (t) for various fire powers (sizes) Q inside buildings of (a), (b) $H = 60$ m, (c), (d) $H = 120$ m, and (e), (f) $H = 240$ m. The left and right columns correspond to the all-windows-closed and all-windows-open cases, respectively.

revealed for smaller-scale fires in Figs. 7 and 9, under the conditions of all-closed and all-open windows, respectively.

Fig. 13 compares the temperature T and velocity w distributions in the all-windows-closed and al-windows-open cases. It should be emphasized that the distributions presented herein are the time-averaged steady-state solutions. It is clear that the smoke dynamics corresponding to the closed-windows case revealed higher velocities at the same fire power because the flow in this case exhibited the characteristics of a shaft flow with only one inlet and one outlet. However, when all windows were open, the flow inside resembled a plume flow under open-air conditions, which facilitates suction of cold air into plume and thus diminishes the buoyancy force and decelerates the flow. As a result, both temperature T and velocity w are diminished in the open-windows case in comparison with the closed-windows case. Although the temperature T distribution was relatively uniform on each floor, the velocity w distribution exhibited a zigzag or alternating pattern determined by the repetition of acceleration and deceleration near the corners of the stairwell.

When the fire power Q increased, both T and w increased because they acquired a higher-power source thermal energy and thus, were by-products of a higher buoyancy force. In principle, the temperature could be as high as 1000 °C (Fig. 12a, c, and e), although T of about 300 °C in some regions (Fig. 13a), and a maximum velocity of 4 m/s were observed here (Fig. 13b). When $Q \leq 5$ MW, the temperature at the top floor was virtually at the level of room temperature (Fig. 13a). However, smoke reached the top floor because velocity w was sufficiently high even at this relatively low fire power (Fig. 13b). As a rough estimate, the smoke traveled at speeds greater than 1 m/s when $Q \geq 2$ MW. Accordingly, it took less than 10^2 s for smoke to reach the end at a height of 10^2 m. This rapid smoke motion is certainly threatening to human life.

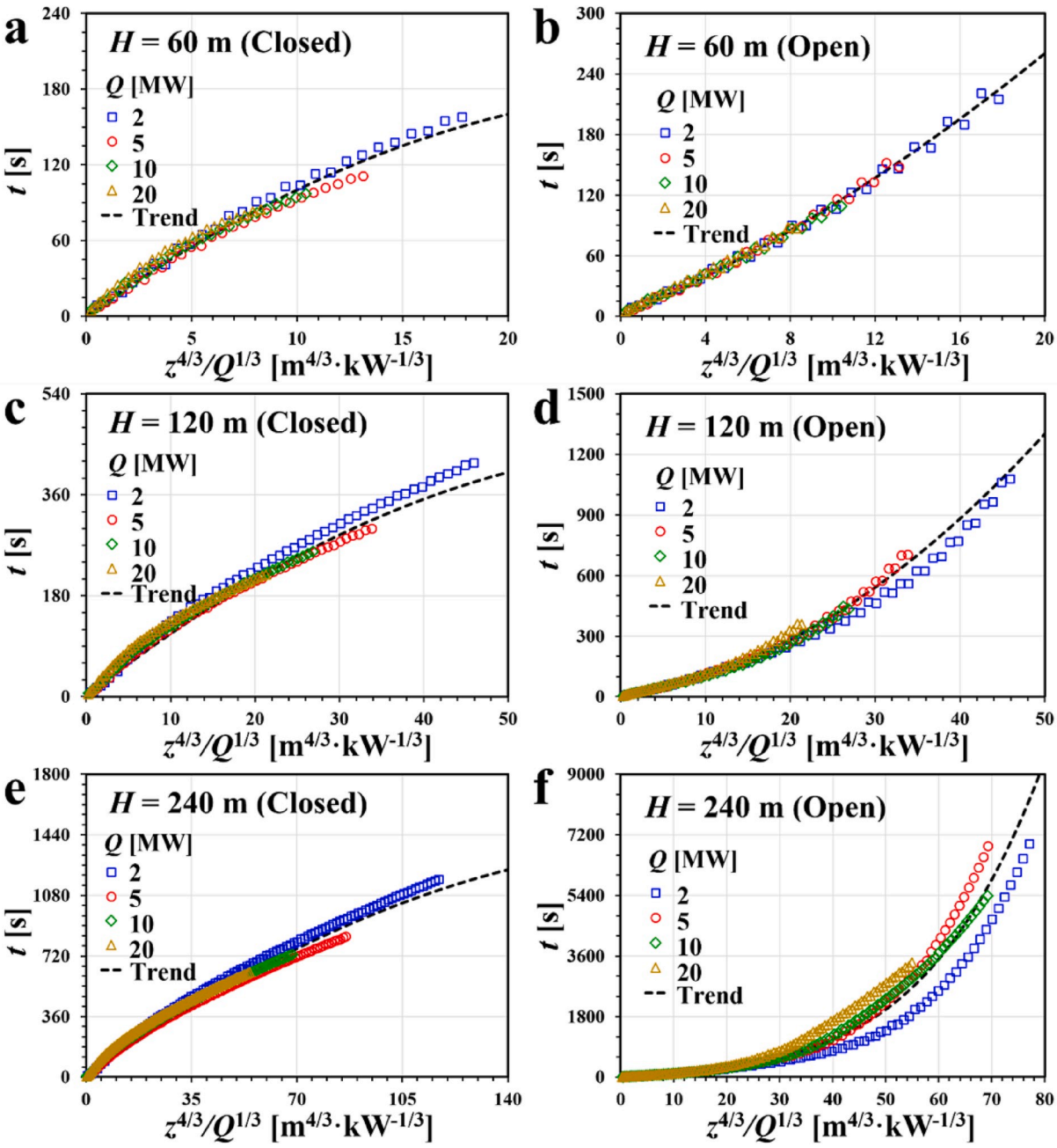

Fig. 17. Smoke rising time with a scaled horizontal axis for data collapse.

Table 1
Values of the constants C_1 and C_2 in Eq. (12) at different building heights.

H [m]	Closed		Open	
	C_1	C_2	C_1	C_2
60	15	0.8	7	1.2
120	19	0.8	1.2	1.8
240	25	0.8	0.005	3.3

Although the smoke temperature was not life-threatening at the top floors, the smoke itself, with its great mobility, is dangerous.

Fig. 14 shows the pressure and density distributions for the all-windows-closed and all-windows-open cases. Overall, the difference between the maximum and minimum pressure was nearly $\Delta P = 15$ Pa, which is high enough to cause a moderate pressure-driven flow. Fig. 14a ascertains the differences between the two cases. When the windows were closed (left), the pressure distribution inside the stairwell was similar to that in a typical shaft flow, which is dominated by the stack effect. A low-pressure region is formed at the low levels because of the buoyancy force (generated by fire), which heats up and lifts air. The low pressure at the fire source draws in more fresh air. On the other hand, the heated air is buoyant but experiences cooling because of the heat transfer into the building walls. As a result, smoke is densified, and the pressure increases toward higher floors. This pushing force is sufficiently high to release smoke into an open atmosphere outside (at $P = 0$ Pa, the gauge pressure). In the open-windows case (right), the pressure distribution between floors did not differ significantly; however, pressure alternated at the stairwell at the same level because of the swirling vortical smoke motion. Such velocity alternation caused the pressure variation. In the open-window case in Fig. 14a, the smoke flow was similar to a plume flow under open-air conditions, and thus, the typical shaft flow characteristic of the stack effect was absent.

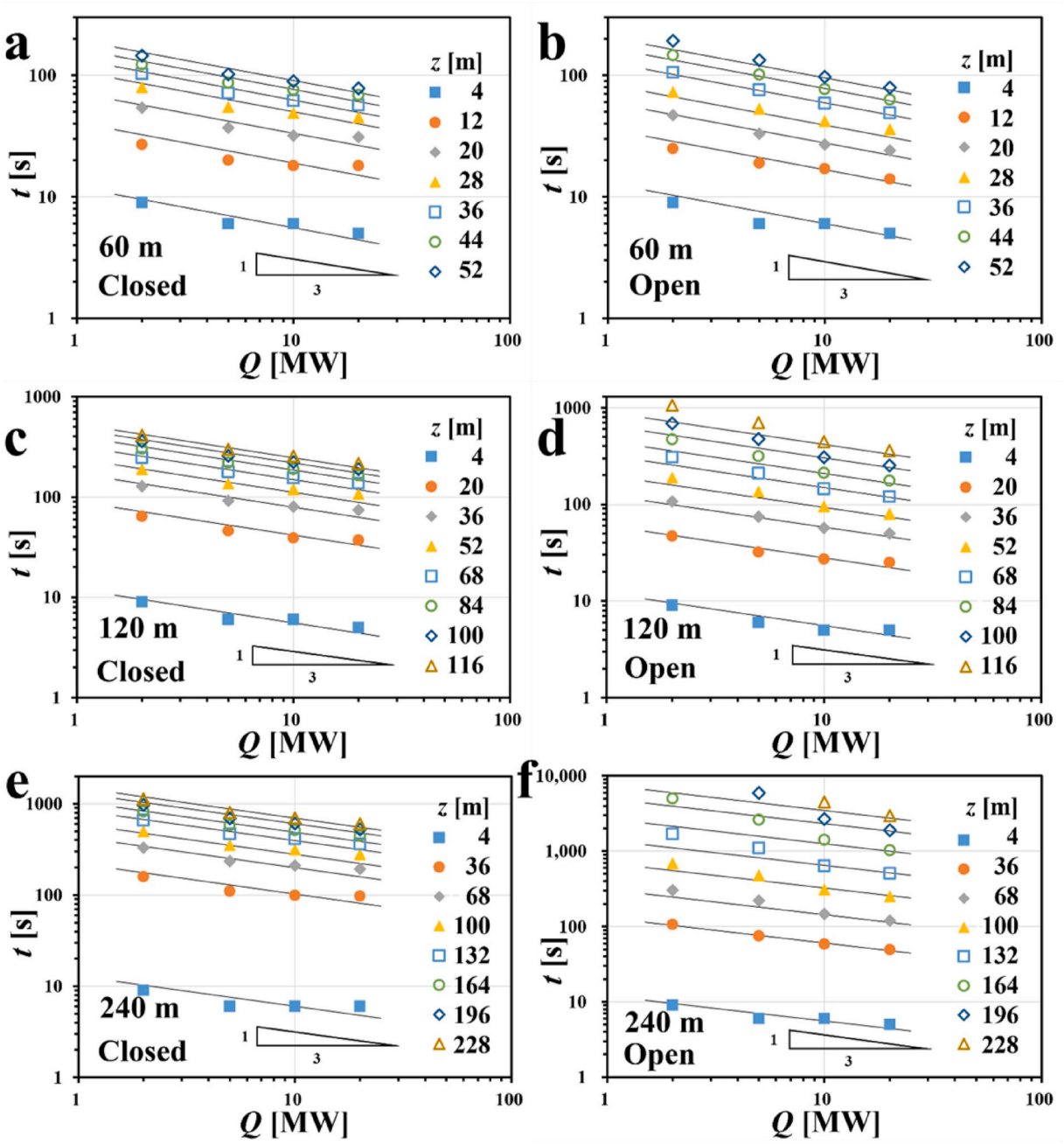

Fig. 18. Log–log plots of t versus Q for (a) 60-m, all-closed; (b) 60-m, all-open; (c) 120-m, all-closed; (d) 120-m, all-open cases; (e) 240-m, all-closed; (f) 240-m, all-open. The scaling exponent of -1/3 shown for comparison is based on the plume theory for an open-air surrounding.

Fig. 14b shows that the density distributions of the closed-window and open-window cases were quite similar, except for some minor details inside the corridor and middle room through which fresh air was supplied when the windows were open. This density distribution was consistent with the temperature distribution in Fig. 13a. The smoke density was higher at higher floors because temperature was lower, which densified air. Conversely, the smoke density was lower at lower floors because the temperature was higher there, which expanded air and lowered its density.

Fig. 15 shows cross-sectional view of the 120-m building at the 15th and 16th floors with the instantaneous trajectories of smoke flow inside the corridor, middle room, and stairwells spaces. The alternating patterns of the flow shown in Figs. 13 and 14 are the direct result of the vortical structure manifested by the streamlines in Fig. 15a. The complex internal geometry inside the building induced several vortices not only near the stairwells but also near ceilings, doors, and windows. This vortical smoke structure shown in Fig. 11 was visualized using the LIF (laser-induced fluorescence) method. It shows that fresh air is supplied through the windows and, at the same time, smoke also escapes through the windows, which is responsible for the vortical flow structure. This phenomenon was also predicted numerically; cf. Fig. 15b. In addition, the temperature distribution presented in Fig. 15c confirms that the rising hot smoke undergoes cooling when moving from the low to higher floors. A cooler air is supplied through the hallway bottom from the open windows and the hot smoke escapes from the stairwell to the windows through the upper half of the hallway. In Fig. 15d, the heavier cooler air is present in the lower half of the hallway, while the lighter hotter smoke is presents in the upper half of the hallway.

The alternating flow field was induced through the alternating structure of the stairwells, as shown in Fig. 15a. Therefore, the flow

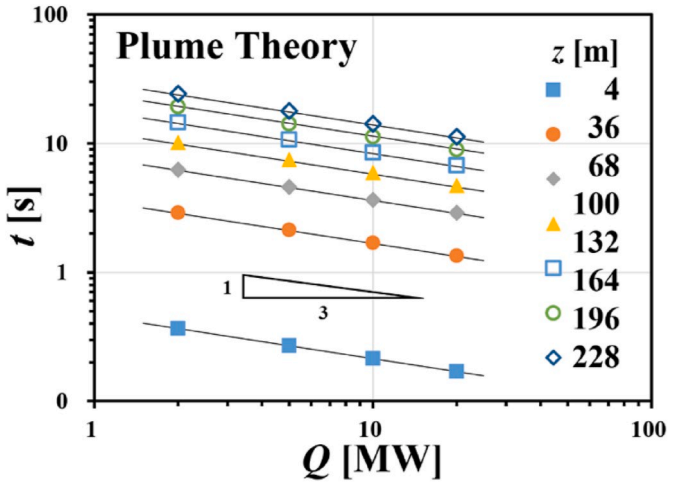

Fig. 19. Log–log plots of t versus Q in comparison with the plume theory with the scaling exponent of -1/3. Note that the plume theory is based on an open-air surrounding.

inside the stairwell column was completely three-dimensional, which is visually confirmed in Movie S1. The smoke was spreading not only in the vertical direction but also in the spanwise and helical directions. As a result, one should keep in mind that the smoke rise time is longer in a complex building than that in an open-air structure or in a silo with no obstructions present.

4.6. Smoke rising time

Fig. 16 compares the smoke rising time (t) for various fire powers (sizes) Q when all windows are closed and open, where the first, second, and third row correspond to building heights of $H = 60$, 120, and 240 m, respectively. Clearly, t was much longer when all windows were open for all building heights because the rising smoke lost momentum for an increased suction of fresh air. Furthermore, when Q was larger due to a greater heating power, the fire-produced buoyancy force was higher and thus t was shorter, as the smoke rapidly reached the top of the building. This pattern is revealed in Fig. 16 for all building heights in both the closed-window and open-window cases. Overall, for a fire power in the $Q \geq 2$ MW range, when all windows were open, the smoke rising time was approximately $t = 10^2$ s for $H = 60$ m; $t = 10^3$ s for $H = 120$ m, and $t = 10^4$ s for $H = 240$ m. For a fire power in the $Q \geq 2$ MW range, when all windows were closed, the smoke rising time was approximately $t \leq 150$ s for $H = 60$ m, $t \leq 400$ s for $H = 120$ m, and $t \leq 1200$ s for $H = 240$ m.

Fig. 17 shows the collapsed data of Fig. 16 plotted versus $z^{4/3}{\cdot}Q^{-1/3}$ to yield an empirical formula that estimates the smoke rising time, t, for various building heights H and fire powers Q. The exponents of -1/3 and 4/3 for Q and z, respectively, were first adopted from Ahn et al. [8–10], but were later modified with the constants, C_1 and C_2 to present an averaged dashed line for various cases in Fig. 17 as

$$t = C_1 \left(\frac{z^{4/3}}{Q^{1/3}} \right)^{C_2} \tag{12}$$

It should be emphasized that the units of z are [m], the Q unit [kW], and the constant C_1 for each height is listed in Table 1, where the data in the first and second columns correspond to the closed-window and open-window cases, respectively. The data collapse shown in Fig. 17 provides a simple empirical formula that can be used to roughly estimate the smoke rising time per given building height. Obviously, it takes longer for smoke to reach the building top in the all-windows-open case because smoke entrains an additional fresh intake air. Therefore, the time range in the vertical axes in Fig. 17b, d, and f (the open-windows case) is much larger than that in Fig. 17a, c, and e (the closed-windows case).

Ji et al. [35] reported the slope of the difference of the smoke rising time (t) on the fire power (Q) on a log–log scale plot for smoke flow inside closed stairwells. They found that the slope was approximately -1/3, which yields the scaling $t \sim Q^{-1/3}$ for the building height of $H = 12$ m. Fig. 18 reveals a trend similar to the scaling of Ji et al. [35] for the smoke rising time with respect to the fire power in the $2 \leq Q \leq 20$ MW range. The exponent in the power-law here is approximately the same as that reported by Ji et al. [35].

Overall, the smoke rising time was longer in the open-window cases than that in the closed-window cases for all locations except $z = 4$ m for the building heights of $H = 60$, 120, and 240 m. At the lowest floors ($z = 4$ m), no difference in t was noted between the closed- and open-window cases. However, the value of t increased significantly for the open-window cases because the fresh intake air slowed down the ascending smoke flow. In the open-window cases, the data deviated from the fitting lines, as seen in the cases of $z \geq 52$ m, $z \geq 84$ m, and $z \geq 132$ m in Fig. 18b, d, and f, respectively, at low fire powers of $Q = 2$ and 5 MW. Thus, one should be aware that the rough estimate based on the fitting lines is inapplicable when the building is tall, and the fire power is low. Because the fitting significantly underpredicted the smoke rising time, either experimental data or numerical simulation must be used for a reasonably accurate prediction in such a case.

Fig. 19 shows the scaling corresponding to the plume theory, which predicts the exponent of -1/3, as per integration of the following kinematic equation

$$\frac{dz}{dt} = w_{\max}(z) = \left(\frac{\beta g Q}{\rho c z} \right)^{1/3}, \tag{13}$$

where β is the thermal expansion coefficient of the gas, c is the specific heat of the gas at constant pressure, ρ is the gas density, and g is the gravity acceleration. Equation (13) yields after integration: $t = (3/4){\cdot}z^{4/3}{\cdot}(\rho c)^{1/3}{\cdot}(\beta g)^{-1/3}{\cdot}Q^{-1/3}$ which reveals that $t \sim z^{4/3}$ and $t \sim Q^{-1/3}$. The dependence of t on Q is plotted in Fig. 19. The slope is -1/3 for all z values and thus $t \sim Q^{-1/3}$. The latter shows that the smoke rising time predicted by the plume theory is in full agreement with the present numerical results under the open-air conditions. That was also reported by Ji et al. [35], albeit their stairwells were inside a closed column, which makes their conclusion quite remarkable. Despite the dramatic difference in the surroundings between the open-air plume and stairwell flows, all these cases are still described by the same scaling of t on Q with the exponent of -1/3. However, this does not mean that the smoke rising time during building fires can be accurately predicted by the plume theory. As the comparison of Figs. 18 and 19 shows, the magnitude of t predicted by the plume theory is significantly smaller than that of the building fires.

5. Conclusion

The smoke dynamics in a confined building under various open-window scenarios were studied numerically and experimentally in model experiments. The numerical results are in good agreement for the smoke dynamics in a prototype building 2 m in height used in the model experiment. This validation allowed us to extend the numerical simulations to an actual-scale fire power of $2 \leq Q \leq 20$ MW. In the latter simulations it was found that the smoke rising time was much shorter for the all-windows-closed case than that for the all-windows open case. The smoke motion was slowed when the amount of intake air through open windows was significant. We found that the smoke rising time depends on the power Q according to the power-law with the exponent of -1/3 irrespective of the building size when all windows were closed. When all windows were open, the smoke rising time increased because of the slowed motion with air intake.

This relation is essentially the same as the one predicted by the plume theory, which is related to an open-air fire scenario. Therefore,

fires in both closed buildings and open-air structures exhibit similar smoke rising time characteristics. However, one should be aware that the magnitude of t predicted by the plume theory is significantly smaller than that of the building fires, rendering a conservative estimate for the smoke rising time. These findings can be useful for fire safety engineers who seek to estimate smoke rising times.

Although the experimental and numerical studies in the present work revealed that the smoke motion was slowed with opening windows, the present work does not suggest that opening a window is favorable for real fire-fighting scenarios because opening it would intensify fires by providing more oxygen. It should be emphasized that some caution should be taken in interpreting the present findings.

Acknowledgement

This work was supported by a grant (20AUDP-B100356-06) from Urban Architecture Research Program primary funded by Ministry of Land, Infrastructure and Transport of South Korean government. And also supported by grants (NRF-2013R1A5A1073861 and NRF-2016M1A2A2936760) from Advanced Research Center Program funded by the National Research Foundation of the South Korea government.

Appendix A. Supplementary data

Supplementary data to this article can be found online at https://doi.org/10.1016/j.ijthermalsci.2020.106500.

References

[1] P. Brennan, Victims and survivors in fatal residential building fires, Fire Mater. 23 (1999) 305–310.
[2] S.i. Sugahara, H. Yoshioka, S. Barua, Case studies of high-rise building fires in dhaka city with reference to building fire code of Japan, Fire Sci. Technol. 30 (2011) 69–80.
[3] D. Winberg, International Fire Death Rate Trends, 2016.
[4] A. Wilson, G.T. Tamura, Stack effect in buildings, in: Canadian Building Digests, vols. 101–150, 1968, 4-4.
[5] R.E. Barrett, D.W. Locklin, A computer technique for predicting smoke movement in tall buildings, Fire Technol. 5 (1969) 299–310.
[6] G.T. Tamura, Computer Analysis of Smoke Movement in Tall Buildings, Division of Building Research, National Research Council, 1969.
[7] A. Wilson, G. Shorter, Fire and high buildings, Fire Technol. 6 (1970) 292–304.
[8] C.-S. Ahn, B.-H. Bang, M.-W. Kim, T.-G. Kim, S.C. James, A.L. Yarin, S.S. Yoon, Numerical investigation of smoke dynamics in unconfined and confined environments, Int. J. Heat Mass Tran. 127 (2018) 571–582.
[9] C.-S. Ahn, B.-H. Bang, M.-W. Kim, S.C. James, A.L. Yarin, S.S. Yoon, Theoretical, numerical, and experimental investigation of smoke dynamics in high-rise buildings, Int. J. Heat Mass Tran. 135 (2019) 604–613.
[10] C.-S. Ahn, C.-W. Park, M.-W. Kim, T.-G. Kim, S.C. James, Y. Yoon, A.L. Yarin, S. S. Yoon, Experimental and numerical investigation of smoke dynamics in vertical cylinders and open-air environment, Int. J. Heat Mass Tran. 135 (2019) 985–995.
[11] L.P. Yarin, The Pi-Theorem: Applications to Fluid Mechanics and Heat and Mass Transfer, Springer-Verlag, Berlin, Heidelberg, 2012.
[12] B. McCaffrey, Purely Buoyant Diffusion Flames: Some Experimental Results. Final Report, Chemical and Physical Processes in Combustion, The National Institute of Standards and Technology (NIST), Miami Beach, 1979, p. 49.
[13] W. Baines, J. Turner, Turbulent buoyant convection from a source in a confined region, J. Fluid Mech. 37 (1969) 51–80.
[14] E.E. Zukoski, Prediction of Smoke Movement in Buildings, California Institute of Technology, Pasadena, California, 1976, p. 91125.
[15] M.G. Worster, H.E. Huppert, Time-dependent density profiles in a filling box, J. Fluid Mech. 132 (1983) 457–466.
[16] S.J. Barnett, The Dynamics of Buoyant Releases in Confined Spaces, University of Cambridge, 1992.
[17] S.S. Cardoso, A.W. Woods, Mixing by a turbulent plume in a confined stratified region, J. Fluid Mech. 250 (1993) 277–305.
[18] M. Wells, R. Griffiths, J. Turner, Competition between distributed and localized buoyancy fluxes in a confined volume, J. Fluid Mech. 391 (1999) 319–336.
[19] J.G. Quintiere, Fire behavior in building compartments, Proc. Combust. Inst. 29 (2002) 181–193.
[20] Y. Chen, X. Zhou, Z. Fu, T. Zhang, B. Cao, L. Yang, Vertical temperature distributions in ventilation shafts during a fire, Exp. Therm. Fluid Sci. 79 (2016) 118–125.
[21] N. George, A. Ooi, K. Moinuddin, G. Thorpe, I. Marusic, D. Chung, Direct Numerical Simulation of a Turbulent Line Plume in a Confined Region, 2016.
[22] X. Gao, A. Li, C. Yang, Study on thermal stratification of an enclosure containing two interacting turbulent buoyant plumes of equal strength, Build. Environ. 141 (2018) 236–246.
[23] L.Y. Cooper, Simulating Smoke Movement through Long Vertical Shafts in Zone-type Compartment Fire Models, National Institute of Standards and Technology, Building and Fire Research Laboratory, 1998.
[24] S.Y. Kim, Y. Jaluria, Basic considerations in combined buoyancy-induced and forced flow in a vertical open shaft, Numer. Heat Tran. 34 (1998) 519–536.
[25] G. Mercier, Y. Jaluria, Fire-induced flow of smoke and hot gases in open vertical enclosures, Exp. Therm. Fluid Sci. 19 (1999) 77–84.
[26] T. Tanaka, T. Fujita, J. Yamaguchi, Investigation into rise time of buoyant fire plume fronts, International Journal on Engineering Performance-Based Fire Codes 2 (2000) 14–25.
[27] J. Zhang, J. Ji, R. Huo, H. Yuan, R. Yang, A comparison of simulation and experiment on stack effect in long vertical shaft, J. Fire Sci. 24 (2006) 121–135.
[28] G. Xiao, J. Tu, G. Yeoh, Numerical simulation of the migration of hot gases in open vertical shaft, Appl. Therm. Eng. 28 (2008) 478–487.
[29] X. Sun, L. Hu, W. Chow, Y. Xu, F. Li, A theoretical model to predict plume rise in shaft generated by growing compartment fire, Int. J. Heat Mass Tran. 54 (2011) 910–920.
[30] R. Harish, K. Venkatasubbaiah, Transport phenomena of turbulent fire spread through compartment connected to vertical shaft in tall building, Fire Saf. J. 61 (2013) 160–174.
[31] D. Qi, L. Wang, R. Zmeureanu, Modeling smoke movement in shafts during high-rise fires by a multizone airflow and energy network program, Build. Eng. 121 (2015).
[32] D. Qi, L. Wang, R. Zmeureanu, The effects of non-uniform temperature distribution on neutral plane level in non-adiabatic high-rise shafts during fires, Fire Technol. 53 (2017) 153–172.
[33] J. Zhang, W. Lu, R. Huo, R. Feng, A new model for determining neutral-plane position in shaft space of a building under fire situation, Build. Environ. 43 (2008) 1101–1108.
[34] X. Sun, L. Hu, Y. Li, R. Huo, W. Chow, N. Fong, G.C. Lui, K. Li, Studies on smoke movement in stairwell induced by an adjacent compartment fire, Appl. Therm. Eng. 29 (2009) 2757–2765.
[35] J. Ji, L. Li, W. Shi, C. Fan, J. Sun, Experimental investigation on the rising characteristics of the fire-induced buoyant plume in stairwells, Int. J. Heat Mass Tran. 64 (2013) 193–201.
[36] L. Li, J. Ji, C. Fan, J. Sun, X. Yuan, W. Shi, Experimental investigation on the characteristics of buoyant plume movement in a stairwell with multiple openings, Energy Build. 68 (2014) 108–120.
[37] D. Qi, L. Wang, R. Zmeureanu, An analytical model of heat and mass transfer through non-adiabatic high-rise shafts during fires, Int. J. Heat Mass Tran. 72 (2014) 585–594.
[38] W. Shi, J. Ji, J. Sun, S. Lo, L. Li, X. Yuan, Influence of fire power and window position on smoke movement mechanisms and temperature distribution in an emergency staircase, Energy Build. 79 (2014) 132–142.
[39] W.X. Shi, J. Ji, J.H. Sun, S. Lo, L.J. Li, X.Y. Yuan, Experimental study on influence of stack effect on fire in the compartment adjacent to stairwell of high rise building, J. Civ. Eng. Manag. 20 (2014) 121–131.
[40] J. Ji, M. Li, Y. Li, J. Zhu, J. Sun, Transport characteristics of thermal plume driven by turbulent mixing in stairwell, Int. J. Therm. Sci. 89 (2015) 264–271.
[41] J. Ji, H. Wan, Y. Li, K. Li, J. Sun, Influence of relative location of two openings on fire and smoke behaviors in stairwell with a compartment, Int. J. Therm. Sci. 89 (2015) 23–33.
[42] L. Li, J. Ji, W. Shi, Z. Gao, J. Sun, J. Zhu, A modified turbulent mixing model with the consideration of heat transfer between hot buoyant plume and sidewalls in a closed stairwell, Int. J. Heat Mass Tran. 84 (2015) 521–528.
[43] J. Ji, M. Li, Z. Gao, Y. Li, W. Shi, J. Sun, Experimental investigation of combustion characteristics under different ventilation conditions in a compartment connected to a stairwell, Appl. Therm. Eng. 101 (2016) 390–401.
[44] J. Ji, M. Li, W. Shi, Z. Gao, J. Sun, S. Lo, Deflection characteristic of flame with the airflow induced by stack effect, Int. J. Therm. Sci. 115 (2017) 160–168.
[45] M. Li, Z. Gao, J. Ji, K. Li, Modeling of positive pressure ventilation to prevent smoke spreading in sprinklered high-rise buildings, Fire Saf. J. 95 (2018) 87–100.
[46] J. Zhang, J. Weng, T. Zhou, D. Ouyang, Q. Chen, R. Wei, J. Wang, Investigation on smoke flow in stairwells induced by an adjacent compartment fire in high rise buildings, Appl. Sci. 9 (2019) 1431.
[47] R.J. Moffat, Describing the uncertainties in experimental results, Exp. Therm. Fluid Sci. 1 (1988) 3–17.
[48] I.O.f. Standardization, Uncertainty of Measurement-Part 3: Guide to the Expression of Uncertainty in Measurement (GUM: 1995), ISO, 2008.
[49] K.B. McGrattan, H.R. Baum, R.G. Rehm, A. Hamins, G.P. Forney, J.E. Floyd, S. Hostikka, K. Prasad, Fire Dynamics Simulator–Technical Reference Guide, National Institute of Standards and Technology, Building and Fire Research Laboratory, 2000.
[50] J. Ji, Z. Gao, C. Fan, J. Sun, Large Eddy Simulation of stack effect on natural smoke exhausting effect in urban road tunnel fires, Int. J. Heat Mass Tran. 66 (2013) 531–542.
[51] C. Fan, L. Zhang, S. Jiao, Z. Yang, M. Li, X. Liu, Smoke spread characteristics inside a tunnel with natural ventilation under a strong environmental wind, Tunn. Undergr. Space Technol. 82 (2018) 99–110.
[52] H.R. Baum, R.G. Rehm, The equations of motion for thermally driven, buoyant flows, J. Res. Natl. Bur. Stand. 83 (1978) 297–308.
[53] R.S. Rogallo, P. Moin, Numerical simulation of turbulent flows, Annu. Rev. Fluid Mech. 16 (1984) 99–137.

[54] U. Piomelli, Large-eddy simulation: achievements and challenges, Prog. Aero. Sci. 35 (1999) 335–362.
[55] P. DesJardin, L. Gritzo, S. Tieszen, Modeling the effect of water spray suppression on large-scale pool fires, Proceedings (2000) 262–273.
[56] C. Meneveau, J. Katz, Scale-invariance and turbulence models for large-eddy simulation, Annu. Rev. Fluid Mech. 32 (2000) 1–32.
[57] P.E. DesJardin, T.J. O'Hern, S.R. Tieszen, Large eddy simulation and experimental measurements of the near-field of a large turbulent helium plume, Phys. Fluids 16 (2004) 1866–1883.
[58] British S. I.. Application of Fire Safety Engineering Principles to the Design of Buildings: Code of Practice, British Standards Institution, 2001.